UNIVERSITAT POLITÈCNICA DE CATALUNYA

MASTER THESIS

Reduced models to calculate stationary solutions for the lid-driven cavity problem

María Muriel Gracia

SUPERVISED BY

Dr. Adeline de Villardi de Montlaur
Dr. Jose Manuel Vega de Prada

Universitat Politècnica de Catalunya
Master in Aerospace Science & Technology
July 2010

Reduced models to calculate stationary solutions for the lid-driven cavity problem

BY

María Muriel Gracia

DIPLOMA THESIS FOR DEGREE

Master in Aerospace Science and Technology

AT

Universitat Politècnica de Catalunya

SUPERVISED BY:

Dr. Adeline de Villardi de Montlaur
EPSC (UPC)
Dr. Jose Manuel Vega de Prada
ETSI Aeronáuticos (UPM)

ABSTRACT

This Master thesis presents a method that allows for the quick calculation of any steady state solution for flow problems with a Reynolds number within a selected range, namely, for which a steady state is reached.

The method proposed here first requires to calculate various steady state solutions (for appropriate values of the Reynolds number) using a given computational fluid dynamics (CFD) code. These provided solutions are called snapshots and are then used to construct the model based on the combination of proper orthogonal decomposition (POD) and modal interpolation.

This method is applied to the lid-driven cavity problem, which consists in studying the motion of an incompressible fluid inside a squared cavity, whose upper wall moves horizontally. When Reynolds numbers are not too large (for example here up to 10000) the flow converges to a steady state solution.

The method is analyzed in connection with a) the number of snapshots that are needed for a given precision, b) the possibility of using high order singular value decomposition (HOSVD) instead of POD, c) the number of POD/HOSVD modes that must be retained and d) the overall computational efficiency of the reduced order model.

ACKNOWLEDGEMENTS

First of all, I would like to thank Adeline de Villardi and José Manuel Vega for the daily help, support and dedication put in guiding this master thesis.

I am also indebted to Filippo Terragni for providing me with the spectral CFD code to compute the snapshots that have been used along this dissertation, and both Filippo and Luis Santiago Llorente for their help and advices during the last ten months.

In addition, I would like to thank the whole group of PhD students of the ETSI Aeronáuticos (UPM), in particular, Filippo, Robert, Juan Angel, Jose, David and Luis, who received me with opened arms, have made me feel in place at any moment and have always given me a hand when needed.

Finally, thanks to my friends and family for their constant encouragement. In particular, I am deeply indebted to my boyfriend, Álvaro, and my parents, Jesús and Blanca, for their constant support and their infinite patient.

Table of Contents

INTRODUCTION 1

CHAPTER 1. BASICS 3

1.1. Motivation 3

1.2. ROMs 3

1.3. Objectives of the study 4

1.4. Thesis distribution 4

1.5. Results 5

CHAPTER 2. POD AND SVD 7

2.1. Introduction 7

2.2. POD 7
2.2.1. Inner product and norm 7
2.2.2. Mathematical formulation 8
2.2.3. Error of the method 9
2.2.4. Orthogonal projection 10

2.3. SVD 10
2.3.1. Description of the method 10
2.3.2. Error 11

CHAPTER 3. HOSVD 13

3.1. Introduction 13

3.2. Basic concepts 13
3.2.1. Tensor norm 13
3.2.2. Errors 13
3.2.3. Concept of the HOSVD 14

3.3. Methodology of the HOSVD 14

3.4. Errors in HOSVD 17

CHAPTER 4. THE LID-DRIVEN CAVITY PROBLEM 19

4.1. Background 19
4.1.1. Selection of the problem 19
4.1.2. Ideas to be developed 19

4.2. Mathematical formulation 20

4.3. The algorithm 21
4.3.1. Temporal integration 21
4.3.2. Spatial discretization 22

4.4. The steady state solutions 24

4.5. The mesh 25

CHAPTER 5. APPLICATION OF THE POD/SVD MODEL TO THE LID-DRIVEN CAVITY PROBLEM 29

5.1. General concepts and particularization to the problem 29

5.2. Global Error 30
5.2.1. Dependence of the SVD error on the number of snapshots and modes taken 31
5.2.2. Interpolation errors 32
5.2.3. A compromise between the number of snapshots and the number of modes 34

CHAPTER 6. APPLICATION OF THE HOSVD TO THE LID-DRIVEN CAVITY PROBLEM 37

6.1. Application of HOSVD to the lid-driven cavity problem 37

6.2. Global Error 38

6.3. Interpolation error 41

CHAPTER 7. CONCLUISIONS AND FUTURE DEVELOPMENTS 43

7.1. Summary 43

7.2. Conclusions 43

7.3. Future developments 44

References 47

List of Figures

4.1 Lid-driven cavity 20
4.2 Chebyshev-Gauss-Lobatto mesh 23
4.3 Streamlines of the steady state solution (lid driven cavity problem) 25
4.4 Evolution of the maximum error for a 17 x 17 points mesh. 26
4.5 Evolution of the maximum error for a 33 x 33 points mesh 27
5.1 SVD error vs. the number of modes retained (110 snapshots) 31
5.2 SVD error vs. the number of modes retained (110, 36 and 22 snapshots) 32
5.3 RMS and maximum errors resulting from applying SVD + modal interpolation vs. Reynolds number 33
5.4 RMS errors vs. the number of retained modes using 55 equispaced snapshots 34
5.5 RMS errors vs. the number of retained modes using 22 equispaced snapshots 35
5.6 RMS errors vs. the number of retained modes using 11 equispaced snapshots 36
6.1 HOSVD error for the three sets of eigenvalues 39
6.2 Bound for the error for a (2178 x 5 x 11) – tensor 40
6.3 HOSVD + modal interpolation error 42

List of Tables

4.1 Computational time depending on the time step 24
6.1 Table of modes 41
7.1 Time expended by the numerical code 43

INTRODUCTION

Nowadays numerical simulations play an important roll in many industrial sectors, where experiments are being steadily complemented with computational techniques. In particular, in the Aeronautical Industry, the idea of complementing wind tunnel test campaigns with numerical simulations is growing. Of course, wind tunnel experiments will be still needed, at least to validate numerical results.

The main objective of this Master thesis is to develop a model that allows for the quick calculation of the solution of a problem, based on some previous numerical calculations.

To begin with, a set of snapshots needs to be provided (they are calculated using a computational fluid dynamics code) with the steady state solutions for some particular values of the parameter. The model presented is based on a) POD (proper orthogonal decomposition), which provides the best n-dimensional (with n smaller or equal to the dimension of the sample taken) approximation of the solution, and b) modal interpolation. With these techniques, the proposed method calculates an approximation, within a given error, to the solutions corresponding to any value of the parameter.

To test our method, we consider the 2-D lid-driven cavity problem, which consists in the motion of a fluid enclosed in a squared cavity where the upper wall is laterally moved at a constant velocity. This problem is often used as a test example for new codes and has been studied for a long time. It depends only on the Reynolds number (nondimensional parameter). A description of the problem and the code used to numerically solve it are also given in the Master thesis.

The proposed model is compared at the end with a similar model thought for multi-parameter problems.

The method could also be applied to various aerodynamic problems that are of great interest in the Aeronautic Industry. Among these, calculation of aerodynamic loads is an essential ingredient in both design and certification of commercial aircrafts.

Chapter 1

BASICS

1.1. Motivation

During the last decades, experiments in engineering have been steadily complemented with numerical simulations. In fact, nowadays there is (almost) no competitive industry where computational simulations do not play an important role in the design phase. But direct numerical simulation of realistic industrial problems involving fluid dynamics is numerically too expensive and requires huge computational resources, which can be kept reasonable using Reduced Order Models (ROMs). This trend can be easily appreciated in the literature of the past twenty-five or thirty years (see, for instance, references from [1] to [8]).

This trend to substitute experiments by numerical simulations is, in general, due to the flexibility and cost-competitiveness of the latter. In particular, there is a growing trend in the Aeronautic Industry to substitute wind tunnel tests by Computational Fluid Dynamics (CFD) simulations. The first difficulty of CFD is the lack of confidence among designers. The trust gained after using wind tunnel tests cannot be matched to that provided by computational simulations.

Another important problem of CFD is that, despite the advances in computing power, there are still many systems that remain out of reach due to their high dimension. A clear example in the aircraft industry occurs when dealing with aerodynamic databases, which are usually multi-parametric. This means that thousands of simulations can be needed to fill these databases up (see [1]). The main goal of model reduction is to find a lower-dimensional system, which approximates the high-dimensional one retaining as much information as possible; namely, minimizing the error when solving the system. Reduced Order Models (ROMs) provide cost-efficient and reasonably good results in a competitive time.

In fact, both computational efficiency and effectiveness of the method can become crucial factors to improve design cycles, saving both design costs and time. This is why each year the number of published papers containing different reduced order methods and applications increases. Improvement of these two factors should give industry the needed level of confidence for practical applications of CFD, using wind tunnel test only for validation.

1.2. ROMs

As it has been previously mentioned, there are cases where thousands of simulations are necessary to study a design problem. For instance, consider the case of studying the aerodynamic coefficients and surface pressure distribution of a 2-D airfoil depending on Reynolds and Mach numbers, angle of attack and flap deflection angle. If 5 to 10 values for each parameter are considered, between 5^4 to 10^4

simulation runs would be needed; and this without taking into account geometry design parameters or the case where a 3-D wing is considered (see [1], [2] and [3]). It is clear that in this case the cost advantage associated with CFD is eclipsed by the number of simulations needed.

One way to deal with this could be usual interpolation, namely, to compute a well-selected number of cases and then use interpolation. However, interpolation accuracy decreases when either the distance between the available points in the parametric space is not small enough or when many parameters are taken into account. An alternative method was proposed by Bui-Thanh et al. (see [4]) in 2D settings and extended to higher dimensions by Lorente et al. (see [1]). The method consists in first using a reduce order model (ROM), POD or SVD (in 2D) and HOSVD in higher dimensions to obtain a low dimensional model of the set of snapshots, and then in interpolating over the global modes obtained. The main advantage is that interpolation on each mode is a 1D interpolation, which substitutes the higher dimensional interpolation that would be needed in principle. The study made in this Master thesis will be based on this idea.

1.3. Objectives of the study

The goal of the Master thesis is to apply the method developed by Lorente et al. [1] to the lid driven cavity problem. The objective is to first use CFD to calculate the solution of a problem for a set of values of parameters, and then to guess a good-enough approximation of the solution for the remaining values of the parameters in a competitive time.

To begin with, the case where the solutions only depend on one parameter is considered. A deep study is carried out in this one-parameter dependence situation, which will help to the better understanding of the algorithms and methods to be applied.

However, it is well known that most of the problems presented in the Aeronautic Industry (and in many other sectors) have to deal with multi-parametric situations. This is the reason why, although the study begins with the case of one-parameter situation, at the end of the Master thesis we deal with a multi-parametric situation, comparing the results obtained by the previous method with the ones obtained under the assumption that there are more than one parameter to account for.

The application of the method needs to be validated either with experiments or with already known data. In this work, the results have been checked with the problem of the lid-driven cavity. As it will be explained, this configuration is chosen to take the steady state solutions for a given Reynolds number range and simulate the solutions for any other Reynolds in that range.

1.4. Thesis distribution

This thesis dissertation begins with the description of the reduced order models that will be used as part of the method, which as previously commented, will be based on

the application of these models (POD or SVD) plus modal interpolation. Then, a selection of the most energetic of the modes given by the ROM used is made and, finally, some 1D interpolations on these global modes are performed to obtain the required solution.

The importance of these models lies on the fact that it is possible to define a way to find the n-dimensional manifold that is closest (in the root mean square sense) to a set of given solutions (known as the snapshot set) of the problem, among all manifolds of dimension *n*. Such manifold is the one spanned by the *n* most energetic modes obtained from the set of modes applying POD. Thus, POD modes provide a basis of global modes that allow obtaining each snapshot as a linear combination of modes.

This part is studied in chapter 2, were we deal with the main ideas of the reduce order models that will be used in the sequel and in the formulation of Proper Orthogonal Decomposition and Singular Value Decomposition.

Once the ideas of the POD and SVD are clear, a method to deal with multi-parametric situations is explained in chapter 3. This method is called High Order Singular Value Decomposition (HOSVD) and it can be seen as an extension of the Singular Value Decomposition described in the previous chapter.

During these first chapters the mathematical decompositions in which all our study is based are described. These are the more theoretical parts of the Master thesis. However, to validate our analysis we need a physical problem to apply the explained theory, and to study and/or compare the results obtained.

Chapter 4 is divided in two sections. At the beginning, a description of the lid-driven cavity problem is given as well as the reasons to select this problem instead of any other one. In the second part, the main ideas of the code used to calculate the solutions of this problem are given.

The last two chapters deal with the discussion of the results obtained. On the one hand, Proper Orthogonal Decomposition and Singular Value Decomposition apply to 2D tensors (namely, matrices), and are seen to be a method to obtain a good-enough approximation of the solution of the problem decreasing drastically the computational time needed to obtain it. On the other hand we have used High Order Singular Value Decomposition, with the main purpose of comparing the results obtained when considering the problem as one-parameter-dependent with those obtained when solving it with a multi-parameter dependence.

1.5. Results

The model presented is an efficient tool to calculate solutions for a one parameter dependent problem, assuming that previous solutions for some values of the parameter have been provided.

In the case of the lid driven cavity problem, if the numerical code is used, the time spent in the calculation of the steady state solution for a particular Reynolds number

increases with the value of the Reynolds number. For instance, when the Reynolds number is equal to 10, the CPU time needed to obtain the solution is around one minute, while if the Reynolds number is 1000, the CPU time is 11 minutes. In contrast, the reduced model used in this work allows to obtain the steady state solutions for any Reynolds number almost instantaneously, namely around 1.5 CPU seconds.

Finally, when comparing with the method used for the multi-parameter dependent cases, the results obtained are not as good as expected. This is because the method is applied to the same one-parameter problem considered above, introducing an artificial dependence on two parameters considering two scales in the only parameter that is present. Such artificial application has been made just to illustrate the application of the method since no a true multi-parameter problem was available. Introducing a second parameter in the CFD code was out of the scope of the present Master thesis. However, some previous studies on related problems (see [1]) makes us to think that application of HOSVD also provides good results in cases in which the problem is genuinely multidimensional.

Chapter 2

POD AND SVD

2.1. Introduction

Reduced Order Models (**ROMs**) have been for long applied in Fluid Dynamics for data compression (see references from [1] to [7]).

Ideally, we would like to create a model in which the dynamics of the system are captured accurately, but with a low number of degrees of freedom. This will be done applying a reduced order model, based on either the Proper Orthogonal Decomposition (**POD**) or the Singular Value Decomposition (**SVD**).

The method of Proper Orthogonal Decomposition has been used in the fluids community for a long time (see [7]). This decomposition is also known as Principal Component Analysis (**PCA**) or Empirical Orthogonal Functions (**EOF**) in Meteorology or as the Karhunen-Loève expansion in Statistics.

The idea of the method is to obtain a lower dimension approximation of the given sample (usually, made with some solutions of the problem). Actually, what POD pursues is to give the best *n*-dimensional (with *n* less or equal to the dimension sample) approximation. This is achieved by first calculating a set of basis functions (which are called *modes*) from the sample, ordering them with respect to the information of the problem provided (in other words, from more to less energetic modes). Afterwards, the *n* first of these modes are selected and some coefficients (called *amplitudes* of the modes) matched to the original sample are obtained, which gives us a linear system to reproduce the whole sample.

On the other hand, Singular Value Decomposition applies to matrices (instead of to systems of vectors) and can be seen as a way to obtaining the modes satisfying the POD (see [6]) in each dimension of the matrix. SVD was created (see [6] and [7]) to be used for real squared matrices in the 1870s (thanks to the work by Beltrami and Jordan), then some changes were introduced in 1902 by Autonne to make it work for complex square matrices and, finally, it was established for general rectangular matrices in 1939, by Eckart and Young.

2.2. POD

2.2.1. Inner product and norm

The first step is to define the inner product and norm that will be used during the process. Here, unless otherwise stated, we consider the L_2 -inner product and norm (so called usual product and norm).

Due to the physical nature of the considered problem, all variables used here (either being scalars or arrays of any order) have their entries lying in $\mathbb{R}$. Thus, the definition of both the norm and the inner product can be particularized as

$$\begin{aligned} \langle \mathbf{x}, \mathbf{y} \rangle &= \sum_{i=1}^{N} x_i y_i \\ \|\mathbf{x}\|_{L_2} &= \sqrt{\sum_{i=1}^{N} (x_i)^2} \end{aligned} \tag{2.1}$$

where $\mathbf{x} = (x_1, ..., x_N)$ and $\mathbf{y} = (y_1, ..., y_N)$ are vectors living in $\mathbb{R}^N$.

2.2.2. Mathematical formulation

Let us consider a set of *N* snapshots

$$u_1 = u(Re_1) \ , ..., \ u_N = u(Re_N) \tag{2.2}$$

where the i-th snapshot is a vector containing vorticity and stream function values (as it will be explain in chapter 4) in the grid points of a spatial mesh of the steady state solution of the reduced lid driven cavity problem for a given Reynolds number. We need to obtain the orthonormal *POD modes*

$$U_1 \ , ..., \ U_N \tag{2.3}$$

associated with the snapshots **(2.2)**.

The first step is to calculate the self-adjoint matrix *R*, called *covariance matrix*, whose elements are defined as

$$Rij = \langle u_i, u_j \rangle \tag{2.4}$$

in terms of the usual inner product. It is worth remembering that since the entries of the snapshots **(2.2)** are values of the stream function and vorticity of a physical problem, they must be real numbers. This implies that all the entries of *R* are real and then *R* is square, symmetric, and positive definite (provided that the snapshots are linearly independent).

Once we have the covariance matrix, we obtain the eigenvalues $(\lambda_i)^2$, and eigenvectors, α_i, of the matrix *R* , the columns of the matrix A below

$$\Sigma=\begin{pmatrix} (\lambda_1)^2 & & 0 \\ & \ddots & \\ 0 & & (\lambda_N)^2 \end{pmatrix}, \quad (\lambda_1)^2 \geq (\lambda_2)^2 \geq \ldots \geq (\lambda_N)^2$$
$$\mathrm{A}=\begin{pmatrix} \vdots & & \vdots \\ \alpha_1 & \ddots & \alpha_N \\ \vdots & & \vdots \end{pmatrix}, \qquad \text{for } i=1,\ldots,N \tag{2.5}$$

It turns out that the *POD modes* **(2.3)** can be written as

$$U_i = \frac{1}{\lambda_i}\sum_{k=1}^{N} \alpha_i^k u_k \tag{2.6}$$

in terms of the snapshots, where α_i^k denotes the k-th component of the i-th eigenvector of the matrix *R*.

Taking into account that the eigenvectors are orthonormal and the product is the usual one, equation **(2.6)** yields to

$$u_i = \sum_{k=1}^{N} \lambda_k \alpha_k^i U_k \tag{2.7}$$

This provides the original snapshots in terms of the *POD modes*.

2.2.3. Error of the method

Using the definition of the *POD modes* given in **(2.6)**, the truncation in the expression **(2.7)** to *n*<*N* terms yields to the best possible *n*-terms approximation of the snapshots.

An estimate of the truncation error is given by (see [5]):

$$\sum_{i=1}^{N} \left| u_i - \sum_{j=1}^{n} \lambda_j \alpha_j^i U_j \right|^2 = \sum_{j=n+1}^{N} (\lambda_j)^2 \tag{2.8}$$

which means that the root mean square (RMS) error resulting from truncation to *n* modes is

$$Error\ RMS = \sqrt{\frac{1}{N}\sum_{j=n+1}^{N} (\lambda_j)^2} \tag{2.9}$$

Using these definitions, we can select the number of modes needed for the reconstruction of the snapshots for a given error.

2.2.4. Orthogonal projection

Once the number of modes *n* has been selected, the original solution can be reconstructed upon orthogonal projection onto the *n*-dimensional span of the selected POD modes, as

$$u = \sum_{i=1}^{n} a_i U_i \qquad \textbf{(2.10)}$$

The coefficients a_i will be called from now on the *amplitudes* of the *POD modes*. Taking into account that POD modes are orthonormal, the amplitudes can be obtained as

$$a_i = \langle U_i, u \rangle, \quad i = 1, ..., n \qquad \textbf{(2.11)}$$

A physical explanation of the POD modes is that they are those that maximize the energy of the projection. This is the same as saying that they minimize the error resulting from the projection onto the subspace spanned by the modes.

2.3. SVD

2.3.1. Description of the method

The Singular Value Decomposition of a *m* x *n* matrix *Q* allows to write the matrix as $Q = U \cdot \Sigma \cdot V^T$, where the superscript *T* denotes the transpose. In this decomposition, *U* is an *m* x *m* orthogonal matrix whose columns are the eigenvectors of $Q \cdot Q^T$, *V* is an *n* x *n* orthogonal matrix whose columns are the eigenvectors of $Q^T \cdot Q$ and Σ is an *m* x *n* positive definite diagonal matrix containing the singular values of *Q* (namely, the square roots of the strictly positive eigenvalues of either $Q \cdot Q^T$ or $Q^T \cdot Q$). The decomposition is made such that the singular values of *Q* are ordered in descending order.

This decomposition can be written in terms of the elements of *Q* as:

$$Q_{ij} = \sum_{k=1}^{r} \lambda_k u_{ik} v_{jk} \qquad \textbf{(2.12)}$$

where *r* is the rank of the matrix *Q*, λ_k are the singular values (in other words, the elements of the diagonal of Σ) and u_{ik} and v_{jk} are the elements of *U* and *V* respectively.

2.3.2. Error

If the decomposition given in **(2.12)** is truncated to $n < N$ terms, then the RMS error can be obtained as done in section 2.2.2 to obtain the truncation error associated with POD. Namely,

$$Error\ RMS = \sqrt{\frac{1}{N}\sum_{j=n+1}^{r}\left(\lambda_j\right)^2} \qquad \textbf{(2.13)}$$

Chapter 3

HOSVD

3.1. Introduction

In this chapter we consider the extension of SVD to third-order tensors using the High Order Singular Value Decomposition (HOSVD). Higher order tensors are treated similarly.

Tensors of order greater than 2 are very often used mathematical tool to describe many physical behaviours. However, these tensors present some difficulties in connection with SVD that are not encountered when working with matrices. Among others, an important fact to take into account is that the determination of the rank of a third-order tensor is an open problem nowadays (see [8] and [9]).

HOSVD is an extension to third or higher order tensors of SVD (which only applies to second-order tensors as we saw in chapter 2) constructed with care due to the difficulties encountered when working with tensors.

3.2. Basic concepts

3.2.1. Tensor norm

In chapter 2, the L_2-inner product and norm for vectors were used and, as it has been already said, HOSVD applies to third order tensors. Then, hereafter we use an extension of the L_2 norm (called the Fröbenius norm) to tensors. For a tensor *A* of order *m* x *n* x *p*, the Fröbenius norm is defined as

$$\|A\| = \sqrt{\sum_{i=1}^{m}\sum_{j=1}^{n}\sum_{k=1}^{p}\left(A_{ijk}\right)^2} \qquad \textbf{(3.1)}$$

3.2.2. Errors

One of the most important parts of the work carried out here is the study of the errors associated with reconstructing the snapshots. With the use of the Fröbenius norm, it is necessary to be careful when calculating the errors, since the error given by $\left\|A - A_{aprox}\right\|$ will be the *global error in the tensor components*. It is convenient to have the error depending weakly on the mesh when the tensor is obtained discretizing a function. This is done re-scaling the error with the total number of elements in A (say *m* x *n* x *p*) to obtain the root mean square error, namely

$$\text{Error} = \frac{\left\| A - A_{aprox} \right\|}{\sqrt{m\ n\ p}} \tag{3.2}$$

It is important to have this in mind, especially when dealing with tensors of different orders.

3.2.3. Concept of the HOSVD

Consider a *m* x *n* x *p* tensor *A*, with components A_{ijk}. The natural extension of SVD would be to find a decomposition of the form

$$A_{ijk} = \sum_{l=1}^{r} \delta_l u_i^l v_j^l w_k^l \tag{3.3}$$

where u_i^l, v_j^l and w_k^l are the components of three sets of vectors and *r* is defined as the minimum value for which this decomposition is possible. This value *r* is called the *rank of the tensor* and contrary to what happens with matrices, it cannot be determined except for some particular cases (such as the case of *2* x *n* x *n* tensors) (see [8]). In fact, due to the difficulties encountered when dealing with tensors, we need to take special care when constructing algorithms converging to minimal decompositions (see [9]). A less restrictive decomposition has been developed that does not present such difficulties and is known as HOSVD, which is of the form

$$A_{ijk} = \sum_{q=1}^{m_1} \sum_{r=1}^{n_1} \sum_{s=1}^{p_1} \sigma_{qrs} u_i^q v_j^r w_k^s \tag{3.4}$$

where σ_{qrs} are the components of a third-order tensor, known as the core tensor, and $\mathbf{u}^q$, $\mathbf{v}^r$ and $\mathbf{w}^s$ form three sets of orthonormal vectors.

The decomposition given in (3.4) is unique and can be obtained efficiently via repeated POD.

3.3. Methodology of the HOSVD

To begin with we consider the matrices B^1, B^2 and B^3 which components are defined as

$$B_{il}^1 = \sum_{j,k} A_{ijk} A_{ijk} \tag{3.5}$$

$$B_{jl}^2 = \sum_{i,k} A_{ijk} A_{ilk} \tag{3.6}$$

$$B_{kl}^3 = \sum_{i,j} A_{ijk} A_{ijl} \tag{3.7}$$

The three eigenvalue problems associated to these three matrices written in terms of the coordinates as

$$\sum_{j,k,l} A_{ijk} A_{ljk} u_l^q = \alpha_q u_i^q \quad \textbf{(3.8)}$$

$$\sum_{i,k,l} A_{ijk} A_{ilk} v_l^r = \beta_r v_j^r \quad \textbf{(3.9)}$$

$$\sum_{i,j,l} A_{ijk} A_{ijl} w_l^s = \gamma_s w_k^s \quad \textbf{(3.10)}$$

Note that these three matrices are the covariance matrices associated with the POD of the fibers of the tensors along the three sets of indexes. Taking into account that B^1, B^2 and B^3 are symmetric and positive definite, the eigenvalues α_q, β_r and γ_s are nonnegative and the three sets of eigenvectors $\mathbf{u}^q$, $\mathbf{v}^r$ and $\mathbf{w}^s$ can be chosen to be orthonormal systems, namely

$$\sum_i u_i^q u_i^{q'} = \delta_{qq'} \ , \ \sum_q u_i^q u_l^q = \delta_{il} \quad \textbf{(3.11)}$$

$$\sum_j v_j^r v_j^{r'} = \delta_{rr'} \ , \ \sum_r v_j^r v_l^r = \delta_{jl} \quad \textbf{(3.12)}$$

$$\sum_k w_k^s w_k^{s'} = \delta_{ss'} \ , \ \sum_s w_k^s w_l^s = \delta_{kl} \quad \textbf{(3.13)}$$

where δ_{ij} is the Kronëcker delta. The modes $\mathbf{u}^q$, $\mathbf{v}^r$ and $\mathbf{w}^s$ are called *HOSVD modes*.

Denoting the ranks of the systems defined in **(3.8)**, **(3.9)** and **(3.10)**, as $\tilde{m}$, $\tilde{n}$ and $\tilde{p}$, respectively (which is the same as saying that the *n* x *p* system of vectors A_{jk} has rank equal to $\tilde{m}$, the *m* x *p* system A_{ik} has rank $\tilde{n}$ and, finally, the rank of the *m* x *n* system of vectors A_{ij} is $\tilde{p}$), we have $\tilde{m} \le m$, $\tilde{n} \le n$ and $\tilde{p} \le p$.

It is worth rewriting the ideas given above in terms of the adjoint problems given in **(3.8)**, **(3.9)** and **(3.10)**. With this in mind, we fix one of the indices (which means fixing *q* for the first equation, *r* for the second equation, and *s* for the third equation) and define the matrices

$$U_{jk}^q = \frac{1}{\sqrt{\alpha_q}} \sum_i u_i^q A_{ijk} \ , \ q = 1, ..., m \quad \textbf{(3.14)}$$

$$V_{ik}^r = \frac{1}{\sqrt{\beta_r}} \sum_j v_j^r A_{ijk} \ , \ r = 1, ..., n \quad \textbf{(3.15)}$$

$$W_{ij}^s = \frac{1}{\sqrt{\gamma_s}} \sum_k w_k^s A_{ijk} \ , \ k = 1, ..., p \quad \textbf{(3.16)}$$

which is similar to the expression for the POD modes obtained in **(2.6)**.

Invoking **(3.8)**, **(3.9)**, **(3.10)**, **(3.11)**, **(3.12)** and **(3.13)** these matrices must be such that

$$\alpha_q U^q_{jk} = \sum_{j',k'} A_{ijk} A_{ij'k'} U^q_{j'k'} \ , \quad \beta_r V^r_{ik} = \sum_{i',k'} A_{ijk} A_{i'jk'} V^r_{i'k'} \ , \quad \gamma_s W^s_{ij} = \sum_{i',j'} A_{ijk} A_{i'j'k} W^s_{i'j'} \qquad \textbf{(3.17)}$$

$$\sum_{j,k} U^q_{jk} U^{q'}_{jk} = \delta_{qq'} \ , \qquad \sum_{i,k} V^r_{ik} V^{r'}_{ik} = \delta_{rr'} \ , \qquad \sum_{i,j} W^s_{ij} W^{s'}_{ij} = \delta_{ss'} \qquad \textbf{(3.18)}$$

Now we can clearly redefine $\tilde{m}$, $\tilde{n}$ and $\tilde{p}$ as:

- $\tilde{m}$: rank of the *m* (*n* x *p*)-matrices obtained fixing the index i in $\tilde{A}_{ijk}$,
- $\tilde{n}$: rank of the *n* (*m* x *p*)-matrices obtained when fixing j in $\tilde{A}_{ijk}$,
- $\tilde{p}$: rank of the *p* (*m* x *n*)-matrices obtained if we fix the index k in $\tilde{A}_{ijk}$.

We define $(\tilde{m}, \tilde{n}, \tilde{p})$ as the *HOSVD-rank* of the tensor.

If we consider the HOSVD of the tensor A in terms of the HOSVD modes calculated above, we have

$$A_{ijk} = \sum_{q=1}^{\tilde{m}} \sum_{r=1}^{\tilde{n}} \sum_{s=1}^{\tilde{p}} \tilde{A}_{qrs} u^q_i v^r_j w^s_k \qquad \textbf{(3.19)}$$

where the components $\tilde{A}_{qrs}$ form a new third-order tensor that will be called from now on *HOSVD – core tensor* and its dimension is ($\tilde{m}$ x $\tilde{n}$ x $\tilde{p}$), with $\tilde{m} \le m$, $\tilde{n} \le n$ and $\tilde{p} \le p$.

In fact the elements of $\tilde{A}$ are given by

$$\tilde{A}_{qrs} = \sum_{i,j,k} A_{ijk} u^q_i v^r_j w^s_k \qquad \textbf{(3.20)}$$

as obtained multiplying **(3.19)** by u^q_i, v^r_j and w^s_k, and taking into account that the HOSVD modes are orthonormal. If some of the eigenvalues α_q, β_r and/or γ_s vanish it means that the system is redundant and it is possible to define it properly taking off equations without losing information. In this case, strict inequalities happen for $\tilde{m}$, $\tilde{n}$ and $\tilde{p}$; in other words, $\tilde{m} < m$, $\tilde{n} < n$ and/or $\tilde{p} < p$, depending on whether the eigenvalues vanish in the system form by α, β and/or γ. Furthermore, if some of the eigenvalues are small compared to the rest of them, then truncation gives a good approximation of the original solution.

3.4. Errors in HOSVD

Let us now find a bound for the error in a similar way as previously done for POD and SVD.

Using **(3.19)** and taking into account that the HOSVD modes are orthonormal (see **(3.11)**, **(3.12)** and **(3.13)),** the following expressions are obtained

$$\sum_{j,k} A_{ijk} A_{ljk} = \sum_{q,r,s,q'} \tilde{A}_{qrs} \tilde{A}_{q'rs} u_i^q u_l^{q'} \qquad \textbf{(3.21)}$$

$$\sum_{i,k} A_{ijk} A_{ilk} = \sum_{q,r,s,r'} \tilde{A}_{qrs} \tilde{A}_{qr's} v_j^r v_l^{r'} \qquad \textbf{(3.22)}$$

$$\sum_{i,j} A_{ijk} A_{ijl} = \sum_{q,r,s,s'} \tilde{A}_{qrs} \tilde{A}_{qrs'} w_k^s w_l^{s'} \qquad \textbf{(3.23)}$$

Now the expressions **(3.8)**, **(3.9)** and **(3.10)** for the eigenvalues can be written as (for the sake of simplicity only the first one is developed here, its counterparts can be done in the same way)

$$\sum_{q,r,s,q',l} \tilde{A}_{qrs} \tilde{A}_{q'rs} u_i^q u_l^{q'} u_l^{q''} \equiv \sum_{q,r,s} \tilde{A}_{qrs} \tilde{A}_{q''rs} u_i^q = \alpha_{q''} \tilde{u}_i^{q''} \qquad \textbf{(3.24)}$$

This equation is multiplied by $u_i^{q'}$ and add in the index i to obtain

$$\sum_{r,s} \tilde{A}_{q'rs} \tilde{A}_{q''rs} \tilde{u}_i^q = \alpha_{q''} \delta_{q'q''} \qquad \textbf{(3.25)}$$

Following the same procedure for the counterparts obtained from the other two eigenvalue equations and rewriting in a more convenient way, the following (diagonal matrices) equations are found

$$\sum_{j,k} \tilde{A}_{ijk} \tilde{A}_{ljk} = \alpha_i \delta_{il} \qquad \textbf{(3.26)}$$

$$\sum_{i,k} \tilde{A}_{ijk} \tilde{A}_{ilk} = \beta_j \delta_{jl} \qquad \textbf{(3.27)}$$

$$\sum_{i,j} \tilde{A}_{ijk} \tilde{A}_{ijl} = \gamma_k \delta_{kl} \qquad \textbf{(3.28)}$$

and adding **(3.26)** in i, **(3.27)** in j and **(3.28)** in k

$$\sum_{i=1}^{\tilde{m}} \alpha_i = \sum_{j=1}^{\tilde{n}} \beta_j = \sum_{k=1}^{\tilde{p}} \gamma_k = \sum_{i,j,k} \tilde{A}_{ijk} \tilde{A}_{ijk} = \left\| \tilde{A} \right\|^2 \qquad \textbf{(3.29)}$$

Finally, note that the original tensor components A_{ijk} satisfy similar relations obtained using **(3.19)** and the equations **(3.26)**, **(3.27)** and **(3.28)**, to know:

$$\sum_{i=1}^{m}\alpha_i = \sum_{j=1}^{n}\beta_j = \sum_{k=1}^{p}\gamma_k = \sum_{i,j,k} A_{ijk}A_{ijk} = \|A\|^2 \qquad \textbf{(3.30)}$$

where expression **(3.30)** is exactly the same as **(3.29)** when no truncation is applied in **(3.20)**, otherwise

$$\|A-\tilde{A}\|^2 \le \sum_{i=\tilde{m}+1}^{m}\alpha_i + \sum_{j=\tilde{n}+1}^{n}\beta_j + \sum_{k=\tilde{p}+1}^{p}\gamma_k \qquad \textbf{(3.31)}$$

Chapter 4

The lid-driven cavity problem

4.1. Background

4.1.1. Selection of the problem

The lid-driven cavity problem consists in studying the motion of an incompressible fluid inside a squared cavity, whose upper wall moves horizontally in a rigid solid fashion. The selection of the lid driven cavity problem is not casual. This is one of the most CFD-studied fluid flow problems. The reason lies in the simplicity of both its geometry and boundary conditions.

In spite of the simplicity of the lid driven cavity problem, it retains all relevant physical behaviours. Also, its geometrical simplicity makes it easier the experimental calibrations of numerical implementations. For these reasons, the cavity problem is often used as a test for the validation of new codes.

Numerical investigation of the physics of a flow inside lid-driven cavity began with the study of Burggraf (see [10]) in 1966 and has been followed by numerous works during the last forty years, among which it is impossible to forget those carried out by Ghia (see [11]) or Botella and Peyret (see [12]).

4.1.2. Ideas to be developed

The lid-driven cavity reaches a steady state at moderate Reynolds number (the ones that will be considered below). Thus, the steady state at these moderate values of the Reynolds number can be obtained leaving the system evolve, using a numerical code to integrate the time-dependent, incompressible Navier-Stokes equations. The code used here is based on a spectral method. In order to allow to use this spectral method, the constant velocity at the upper wall is smoothed out near the upper lateral corners of the cavity. The time dependent incompressible Navier-Stokes governing equations have been discretized using Chebyshev polynomials. The steady state solutions, called snapshots, are calculated as the final states, which simulates how steady states are reached in physical cavities. This requires that the Reynolds number is not too large, since otherwise steady states are not reached and the final state is time-dependent.

Once we are able to calculate the steady states for any Reynolds number in a given range, two difficulties appear. On the one hand, we face one of the most common problems nowadays in engineering; the problem of storage. During the last years, the study of compression of databases has become a very important branch of study in several fields, among which aeronautical engineering stands out. HOSVD allows a very efficient compression of huge databases [2], especially when these are multidimensional and exhibit redundancies along the various dimensions. On the

other hand, the CPU time-cost (namely, the time needed to reach each the steady state solution) can be very large.

4.2. Mathematical formulation

Even though the study of the lid-driven cavity problem itself is not the main object of this thesis, it is convenient to provide the reader with some basic ideas on both the problem itself and the algorithm used to solve it.

Let us consider a 2D bounded square domain Ω = [0,1] x [0,1], where a fluid is enclosed. This fluid evolves according to the incompressible Navier-Stokes equations:

$$\frac{\partial \mathrm{v}}{\partial t} + (\mathrm{v}\cdot\nabla)\mathrm{v} = -\nabla p + \frac{\Delta \mathrm{v}}{Re}, \qquad \nabla\cdot\mathrm{v} = 0 \tag{4.1}$$

in the domain Ω, where $\mathrm{v} = (u, v)$ is the nondimensional velocity field, *p* is the nondimensional pressure, and *Re* the Reynolds number. The boundary conditions are

$$\begin{aligned} (u,v) &= (F(x),0) \text{ on } \Gamma \\ (u,v) &= (0,0) \text{ on } \Omega - \Gamma \end{aligned} \tag{4.2}$$

where *F* is a real function of *x* and $\Gamma = \{(x,y) \in \partial\Omega :\ y = 1\}$ is the upper wall of the cavity (as seen in figure 4.1).

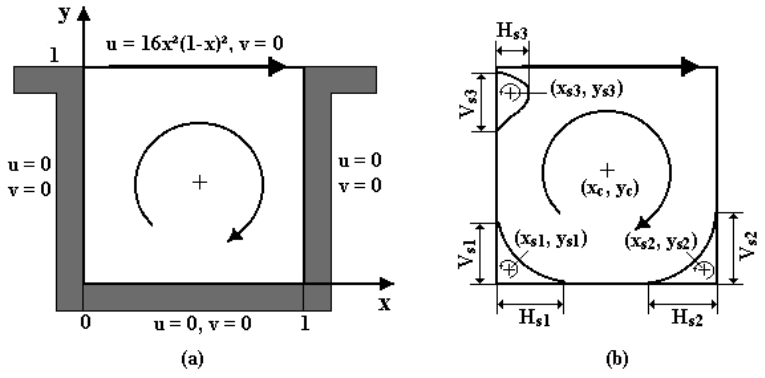

Fig. 4.1 Regularized square lid-driven cavity problem. (a) Boundary conditions. (b) Flow configuration (Tanahashi and Okanaga, 1990**)**

If *F*(x) = 1, then we have the standard lid-driven cavity problem, in which the upper wall moves to the right in a rigid-solid fashion. But such problem exhibits strong singularities near the lateral corners of the upper wall, where the horizontal velocity is discontinuous since it jumps from zero to one. In order to remove these singularities, the following smoothing law for the horizontal velocity distribution is used

$$F(x) = 16x^2(1-x)^2 \tag{4.3}$$

The continuity and Navier-Stokes equations above can be rewritten using the vorticity ω and the stream function ψ as:

$$\omega_t + \psi_y \omega_x - \psi_x \omega_y = \frac{\Delta\omega}{Re} \tag{4.4}$$

$$\Delta\psi = -\omega \tag{4.5}$$

where the subscripts indicate differentiation with respect to the specified variables.

The boundary conditions **(4.2)** are rewritten as

$$\begin{aligned} &\psi = 0 \text{ at } \partial\Omega, \\ &(\partial\psi/\partial x) = 0, \text{ at } x = 0 \text{ and } x = 1 \\ &(\partial\psi/\partial y) = 0, \text{ at } y = 0 \\ &(\partial\psi/\partial y) = F(x), \text{ at } y = 1 \end{aligned} \tag{4.6}$$

The system of the two coupled equations **(4.4)** together with the set of boundary conditions **(4.6)** represent the stream function – vorticity formulation of the regularized lid-driven cavity problem, which can be solved using an spectral algorithm described by Theofilis (see [13]).

4.3. The algorithm

4.3.1. Temporal integration

Temporal integration of **(4.4)** is carried out by a third-order hybrid implicit-explicit three-substep scheme proposed by Sparlat et al. (see [14]).

$$\begin{aligned} \omega' &= \omega^n + \Delta t\left(L(\alpha_1\omega^n + \beta_1\omega') + \gamma_1 N(\omega^n)\right) \\ \omega'' &= \omega' + \Delta t\left(L(\alpha_2\omega' + \beta_2\omega'') + \gamma_2 N(\omega') + \delta_2 N(\omega^n)\right) \\ \omega^{n+1} &= \omega'' + \Delta t\left(L(\alpha_3\omega'' + \beta_3\omega^{n+1}) + \gamma_3 N(\omega'') + \delta_3 N(\omega')\right) \end{aligned} \tag{4.7}$$

where the advance in time is produced from the solution ω^n at time instant $t_n = n\Delta t$ to the solution ω^{n+1} at time instant $t_{n+1} = (n+1)\Delta t$, with $n = 0,1,...$ Here, Δt is the time integration step, and *L* and *N* are the linear and non-linear operators in equation **(4.4)** namely

$$\begin{aligned} L(f) &= \frac{\Delta f}{\mathrm{Re}} \\ N(f) &= \psi_x f_y - \psi_y f_x \end{aligned} \tag{4.8}$$

Note that the linear terms correspond to the viscous part and are treated implicitly while non-linear convective term is treated explicitly.

The parameters in **(4.7)** are chosen such that the method is stable and provides third-order accuracy. The values of these parameters can be found in the work by Sparlat et al. (see [14]).

4.3.2. Spatial discretization

Continuity and momentum equations are spatially discretized using the Chebyshev collocation spectral method. The non-uniform mesh of collocation points is defined on the squared domain Ω = [0,1] x [0,1] considering two sets of Chebyshev-Gauss-Lobatto points:

$$\begin{aligned} \tilde{x}_i &= \cos\left(\frac{i\pi}{N_x}\right), \quad i = 0,...,N_x \\ \tilde{y}_j &= \cos\left(\frac{j\pi}{N_y}\right), \quad j = 0,...,N_y \end{aligned} \tag{4.9}$$

in the *x* and *y* directions, respectively, and then mapping them on the interval [0,1] with a linear transformation, namely

$$\begin{aligned} x_i &= \frac{\tilde{x}_i + 1}{2}, \quad i = 0,...,N_x \\ y_i &= \frac{\tilde{y}_i + 1}{2}, \quad j = 0,...,N_y \end{aligned} \tag{4.10}$$

Thus, we have a mesh (x_i, y_j) of points in the domain Ω = [0,1] x [0,1], with $i = 1,...,N_x$ and $j = 1,...,N_y$.

This discretization is performed (as can be seen in fig. 4.2.) in order to concentrate the mesh points in those regions where dynamics are more complicated, which happens near the walls and especially near the corners of our domain.

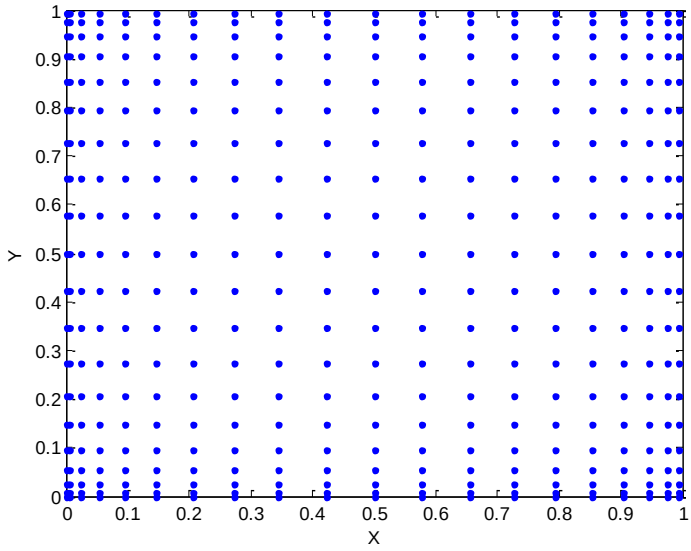

Fig. 4.2 Chebyshev-Gauss-Lobatto mesh with the same number of points in both directions

Concerning the differentiation in the spatial domain, the analytical formulae for derivatives of the Chebyshev polynomials at the Chebyshev-Gauss-Lobatto points yields to the following expression

$$u_i^{'} = \sum_{k=0}^{N_x} (D_x^{(1)})_{ik} u_k \ , \quad i = 0,...,N_x \tag{4.11}$$

where $u_i^{'}$ is the first-order derivative of u with respect to x at collocation point x_i and the operator $D_x^{(1)}$ in matrix form (called *Chebyshev collocation derivative matrix*) accomplishes differentiation in physical space (see [15], [16]) for more details) and is defined as:

$$(D_x^{(1)})_{ij} = \begin{cases} \dfrac{c_i (-1)^{i+j}}{c_j (x_i - x_j)}, & i \neq j \\ -\dfrac{x_j}{2(1-x_j^2)}, & 1 \le i = j \le N_x - 1 \\ \dfrac{2N_x^2 + 1}{6}, & i = j = 0 \\ -\dfrac{2N_x^2 + 1}{6}, & i = j = N_x \end{cases} \tag{4.12}$$

The first order derivative with respect to y at collocation points y_j is defined similarly.

Second order derivatives, both with respect to x and with respect to y and at collocation points x_i and y_j respectively, can be computed as

$$D_{xx}^{(2)} = D_x^{(1)} D_x^{(1)}, \qquad D_{yy}^{(2)} = D_y^{(1)} D_y^{(1)} \tag{4.13}$$

A spectral code to solve the regularized lid-driven cavity problem based on this spectral algorithm is available at the School of Aeronautics, of the Universidad Politécnica de Madrid.

4.4. The steady state solutions

As anticipated above, the flow converges to the steady state solution for Reynolds numbers up to 10000 (see [15]). Although the maximal time step that guarantees the convergence of the method depends on the Reynolds number. Nevertheless, in the case of Reynolds numbers varying in the interval [10, 1100] and with the code used here, it is guaranteed that in order to reach the steady state solution with high precision it is enough to consider $\Delta t = 5 \cdot 10^{-3}$.

Finally, for a given Reynolds number, we consider that the steady state solution is reached when

$$\frac{\max_j \left| \psi_{i+1}^j - \psi_i^j \right|}{\Delta t} < \varepsilon \ , \ and, \ \frac{\max_j \left| \omega_{i+1}^j - \omega_i^j \right|}{\Delta t} < \varepsilon \tag{4.14}$$

where $\varepsilon = 5 \cdot 10^{-9}$.

The CPU time spent to reach the steady state solution, depending on the time step given, is shown in table 4.1. Results are given for different Reynolds numbers and for a grid of 33 x 33 points.

Table 4.1 Computational time (in seconds) depending on the time step

Re	100	500	1000
dt = 0,001	494	1519	2995
dt = 0,005	99	303	600
dt = 0,01	49	152	300

The results obtained for the steady states have been compared with data from literature (see [12]). The streamlines of the steady state solution for different values of Reynolds are shown in figure 4.3. The first plot (top, left) corresponds to Re=100, and shows two very small vortices near the lower corners of the cavity. However, when Reynolds number increases those vortices grow, as seen in the remaining two plots, which correspond to Re= 400 and 1000, respectively. And the main vortex moves to the central part of the cavity.

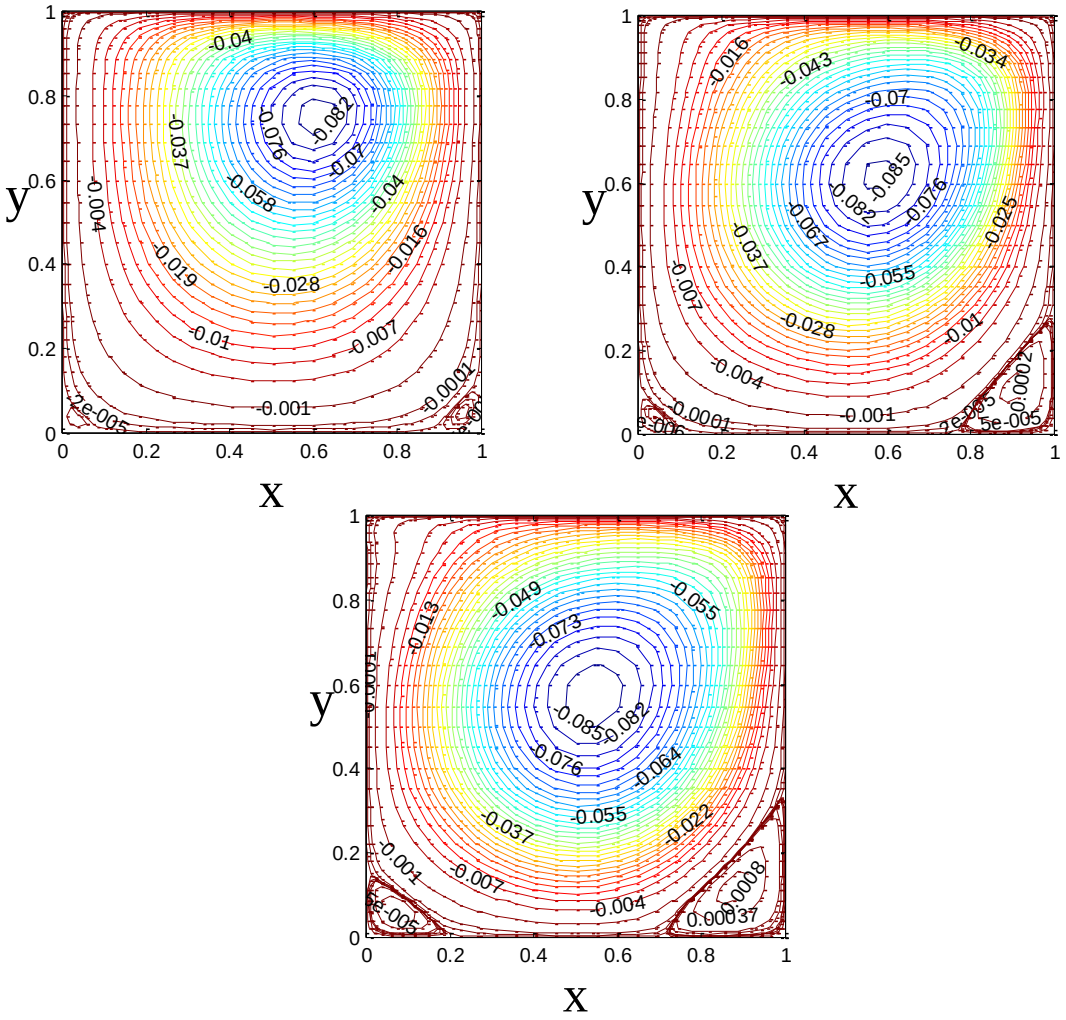

Fig. 4.3 Streamlines of the steady state solution of the lid-driven cavity problem for Reynolds number equal to 100 (top, left), 400 (top, right) and 1000 (bottom).

4.5. The mesh

The number of points on the grid is an important parameter to take into account. On the one hand, if a very thin mesh is selected, then it would lead to very high computational cost. But on the other hand, the mesh must be thin enough to represent well the states of the flow inside the regularized cavity for all the Reynolds numbers in the considered range.

Figures 4.4 and 4.5 show the spatial errors of the time-dependent solution for Reynolds 500. Figure 4.4 shows the maximum error (in logarithmic scale) of the numerical code when working with 17 x 17 mesh-points, as obtained comparing with the results obtained with 33 x 33 mesh-points. As it is observed, the errors for both the horizontal (left plot) and the vertical (right plot) components of the velocity are of the order of 10^{-2}, which is considered a too large error.

In figure 4.5, the maximum spatial errors in a grid of 33 x 33 points are plotted, for both the horizontal (left) and the vertical (right) components of the velocity. In this case, the maximum error is of the order of 10^{-5}, which is considered good enough.

In addition, increasing the number of mesh-points from 17 x 17 to 33 x 33 the time spent by the numerical code to obtain the steady state solutions increases in around a 7.5% and the same happens when increasing from 33 x 33 to 65 x 65 points the mesh. This increment is much smaller than what should be expected estimating the increase in computational cost of the spatial discretization, which would lead to doubling the computational cost. The better performance of the finer mesh is due to the fact that convergence to the steady state solution is faster in the finer mesh, which can be somehow appreciated comparing the plots in figures 4.4 and 4.5.

The results obtained lead us to select the 33 x 33 points grid as the best option to obtain reasonably good accuracy saving computational time and cost.

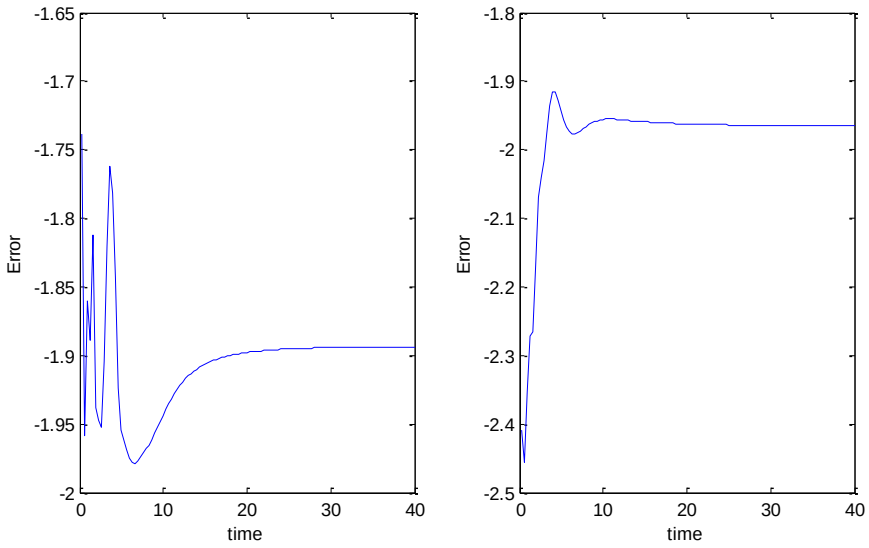

Fig. 4.4 Evolution with time of the maximum spatial error of the method using 17 x 17 mesh-points. Left plot shows the error for the horizontal component *u* of the velocity, while the right plot shows the error for the vertical component *v*. The solution is obtained for Re = 500 and the errors are given in logarithmic scale.

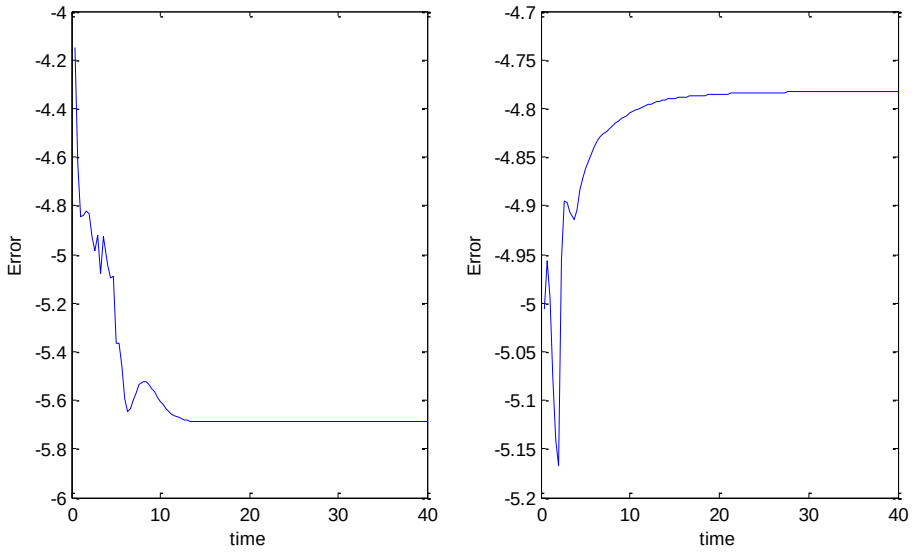

Fig. 4.5 Counterpart of figure 4.2 for the 33x33 mesh

Chapter 5

APPLICATION OF THE POD/SVD MODEL TO THE LID-DRIVEN CAVITY PROBLEM

5.1. General concepts and particularization to the problem

From here on, the decompositions described in chapters 2 and 3 are particularized to the lid-driven cavity problem, described in chapter 4. In particular, this chapter deals with the application of the methods described for the case of one-parameter dependence, using POD and SVD. A model is presented based on these decompositions plus modal interpolation. By modal interpolation we mean interpolation on the parametric modes provided by POD/SVD; spatial modes are common to all values of the parameter, see below.

As anticipated above, the parameter that will be varied is the Reynolds number. However, since only steady states of the problem are considered it requires that the Reynolds number is not too large (less than 10000). In fact, the range selected for the analysis goes from 1 to 1100.

The first ingredient of the model is a set of steady state solutions for some values of the Reynolds number in the above mentioned range. These “on hand” solutions are called the ***snapshots***. Thus, each one of these snapshots, $q(\mathrm{Re})$, is the steady state solution of the lid-driven cavity problem for a given Reynolds number. In other words, the snapshots contain all the stream function and vorticity values at each point of the 33 x 33 points grid selected as seen in the previous chapter.

The snapshots are arranged as vectors providing the 2x33x33 values of the vorticity and stream functions at the 33x33 mesh points. Then a snapshot matrix is constructed whose columns are the snapshots vectors, namely

$$Q = \begin{pmatrix} \vdots & \cdots & \vdots \\ q(\mathrm{Re}_1) & \cdots & q(\mathrm{Re}_N) \\ \vdots & \cdots & \vdots \end{pmatrix} \qquad \textbf{(5.1)}$$

The obtained matrix, Q, is called ***matrix of snapshots***.

Note that this matrix of snapshots is not squared. The number of columns of the matrix is the number of snapshots provided, namely the number of Reynolds numbers that have been selected to calculate the snapshots. The number of rows is twice the amount of points of the grid, once for the stream function values and once for the vorticity. This number (2 x 33 x 33) is independent of the number of snapshots since we have fixed the number of mesh-points.

As a second ingredient, SVD is applied to this matrix, which yields to $Q = U \cdot \Sigma \cdot V^T$. The columns of U and V are the spatial and parametric modes, respectively. This is

because the SVD decomposition can also be written in terms of the components of the snapshots matrix as

$$Q_{ij} \equiv q_i(\mathrm{Re}_j) = \sum_k U_i^k \cdot \lambda_k \cdot V_j^k \qquad \textbf{(5.2)}$$

where the index i accounts for the various spatial mesh points and the index j depends on the Reynolds number. Thus, the modes U depend only on the spatial mesh and the modes V account for the various values of the Reynolds number. The spatial modes are precisely the POD modes that would be obtained applying POD to the set of snapshots considered above. SVD has the additional advantage, as compared to POD, of also providing the parametric modes. In other words, the equation **(5.2)** can also be written as

$$q_i(\mathrm{Re}) = \sum_k U_i^k \cdot \lambda_k \cdot V^k(\mathrm{Re}) \qquad \textbf{(5.3)}$$

This illustrates the fact that if the Reynolds number is varied, both the spatial modes and the singular values remain constant. As a consequence, if an intermediate value of the Reynolds number (different from the ones already considered to calculate the snapshots) is to be accounted for, interpolation must only be made in the parametric modes V. Such one-dimensional interpolation on V^k will be called *modal interpolation* below, and it is the third ingredient of the POD+modal interpolation reduced order model. Namely, the method consists in three steps:

1. Calculate, using the spectral code, a set of snapshots for various representative values of the Reynolds number.
2. Apply SVD to calculate the spatial and parametric modes.
3. Interpolate in the parametric modes. Cubic spline interpolation is applied in the application of the method below.

It is convenient to note that if POD were applied, the method above could be seen as (i) only considering the spatial modes, U^k, (ii) calculating the POD mode amplitudes of the snapshots (obtained projecting the snapshots onto the set of retained POD modes as $q_i(\mathrm{Re}_j) = \sum_k A_k(\mathrm{Re}_j) U_i^k$), and (iii) interpolating in the mode amplitudes. Both ways of proceeding, using either SVD or POD are equivalent because the mode amplitudes are seen to be $A_k(\mathrm{Re}_j) = \lambda_k V_j^k$

5.2. Global Error

It is necessary to distinguish between the different factors that contribute to the error of the model. On the one hand, the error resulting from the SVD is studied. This error depends on both the number of snapshots taken on the interval and the number of modes selected to project the solution. On the other hand, there is an interpolation error.

5.2.1. Dependence of the SVD error on the number of snapshots and modes taken

As seen above, the root mean squared error of truncating the decomposition to n modes, is given by **(2.9)** or **(2.13)**, to remember $\sqrt{\frac{1}{N}\sum_{k=n+1}^{N}(\lambda_k)^2}$, where N is the number of snapshots provided and λ_k are the singular values.

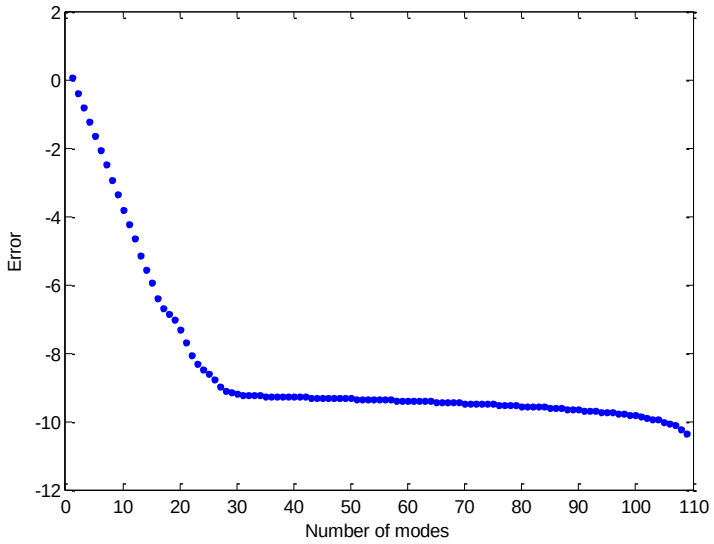

Fig. 5.1 Logarithm of the SVD error vs. the number of modes retained, when 110 snapshots are provided.

The RMS error of the SVD method is represented in figure 5.1, as obtained considering as snapshots the steady state solutions for Reynolds numbers taken from 10 to 10 in the range going from 10 to 1100 (which yields to 110 equispaced snapshots). The plot shows the curve generated by the root mean squared error of the method as the number of modes is varied. Note that the errors fall spectrally until they reach an error of 10^{-9}, which is the order of precision associated with calculating the steady state solution with the numerical code. The shape of the curve, and the fact that the error stabilizes as the number of modes is around 25% of the number of snapshots drive us to think that the number of given snapshots is enough to calculate the solutions for any Reynolds number in this range within a given precision. In fact, a fewer number of snapshots should be enough if these were appropriately chosen, but an automatic efficient method for such selection is not available yet. Of course, such selection could always be made by hand, concentrating snapshots at the upper part of the Reynolds number range, but a systematic selection method would be quite convenient.

Let us now consider the dependence of the SVD error on the number of snapshots, considering that these are equispaced in the Reynolds number range. This is shown in figure 5.2, where the blue line corresponds to the curve plotted in figure 5.1, which is taken as reference, and dots indicate RMS errors when a smaller amount of

snapshots are considered: 36 snapshots obtained for 36 equispaced Reynolds numbers and 22 equispaced snapshots, respectively in the left and right plots. In both cases the error reaches the same minimum level (namely, 10^{-9}) as the number of retained modes is increased.

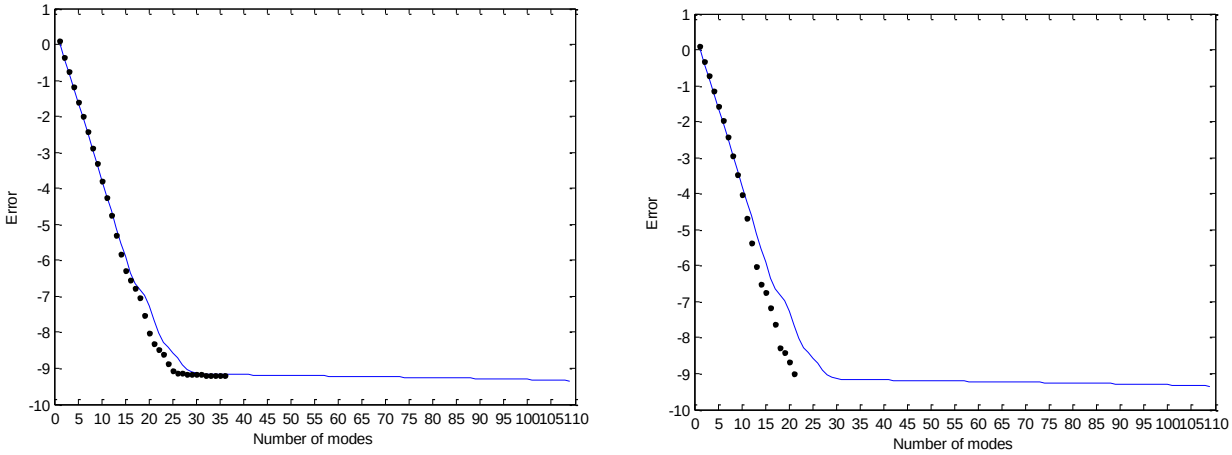

Fig. 5.2 Logarithm of the SVD error vs. the number of retained modes using 110 (blue curve), 36 (dots in left plot), and 22 (dots in the right plot) equispaced snapshots.

Note that as the number of retained modes increases, the error decreases faster if the number of snapshots is smaller. This is somewhat surprising, but it is due to the way in which the SVD error is defined. Namely, the SVD error is the RMS error in reconstructing the snapshots, which decreases as the number of snapshots decreases. Figure 5.2 just shows that this effect is stronger than the one associated with the fact that the quality of the modes increases as the number of snapshots increases; the latter effect would give a trend that is opposite to what is observed in figure 5.2.

5.2.2. Interpolation errors

An approximation of the solution for a Reynolds number in the given range, which does not coincide with one of those for which the snapshot is already available can be obtained by modal interpolation on the parametric modes, as explained above. In order to check interpolation errors, 55 equispaced snapshots (corresponding to $\mathrm{Re} = (2 \cdot k + 1) \cdot 10$ for k=1,2,...) are considered and the solution is reconstructed at the 54 intermediate values of the Reynolds number (namely, $\mathrm{Re} = (2 \cdot k) \cdot 10$, with k=1,2,...), which are taken as test cases. Comparison with the steady state solution, obtained using the spectral code, provides the error of the method; both RMS errors and maximum errors (along the 54 test cases) will be considered. The idea is that, as the number of retained modes is increased, the error converges to the combination of the CFD error and the interpolation error; since the former is quite small, the interpolation error is to be reached. On the other hand, as the Reynolds number

approaches those values associated with one of the snapshots, the interpolation error converges to zero.

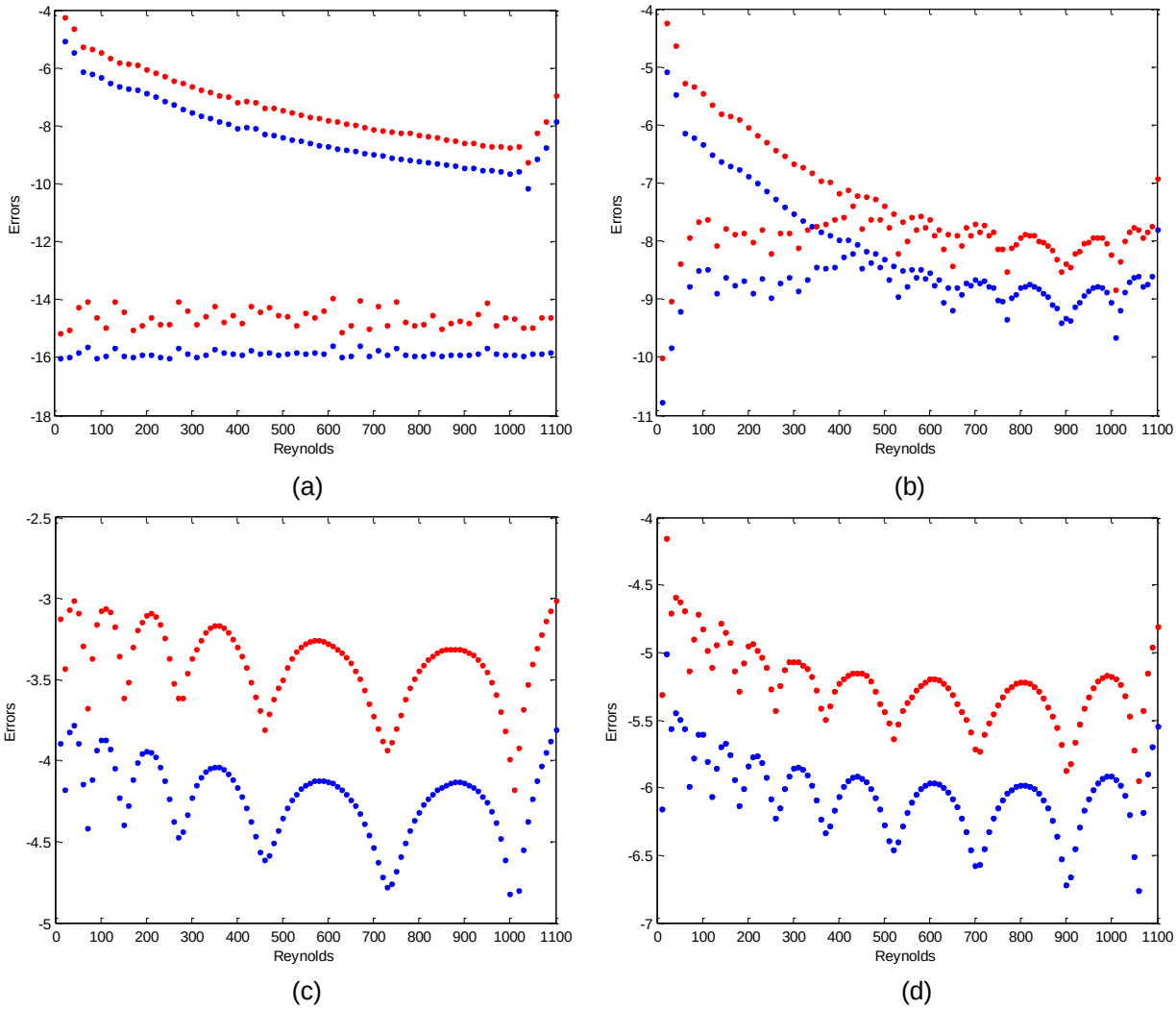

Fig. 5.3 RMS errors (blue dots) and maximum errors (red dots) resulting from applying the SVD+modal interpolation method vs. the Reynolds number, using 55 equispaced snapshots and retaining (a), 28 (b), 12 (c), and 8 (d) spatial modes. The values of the Reynolds number for the 54 test cases (upper curves) and the 55 snapshots (lower curves) are considered.

Figure 5.3 shows the maximum error (in red) and the RMS error (in blue) versus the Reynolds number for both the test cases and the snapshots, retaining four different numbers of modes. If 55 modes are retained, the truncation error due to SVD is negligible, as seen noticing that the lower curves in plot (a) fall to the level of -15. Thus, the upper curves precisely yield to the interpolation errors. If the number of retained modes is decreased, SVD truncation errors increase and become of the same order as the interpolation errors, which is appreciated in plot (b), which corresponds to retaining 28 modes. If the number of retained modes is further decreased, truncation errors dominate and the upper and lower curves (recalled that these corresponds to the test cases and the snapshots, respectively) become

indistinguishable, as seen in plots (c) and (d), which result from retaining 12 and 8 modes, respectively.

5.2.3. A compromise between the number of snapshots and the number of modes

Let us consider a real case, requiring that the maximum error on the stream function and the vorticity is smaller 10^{-3}.

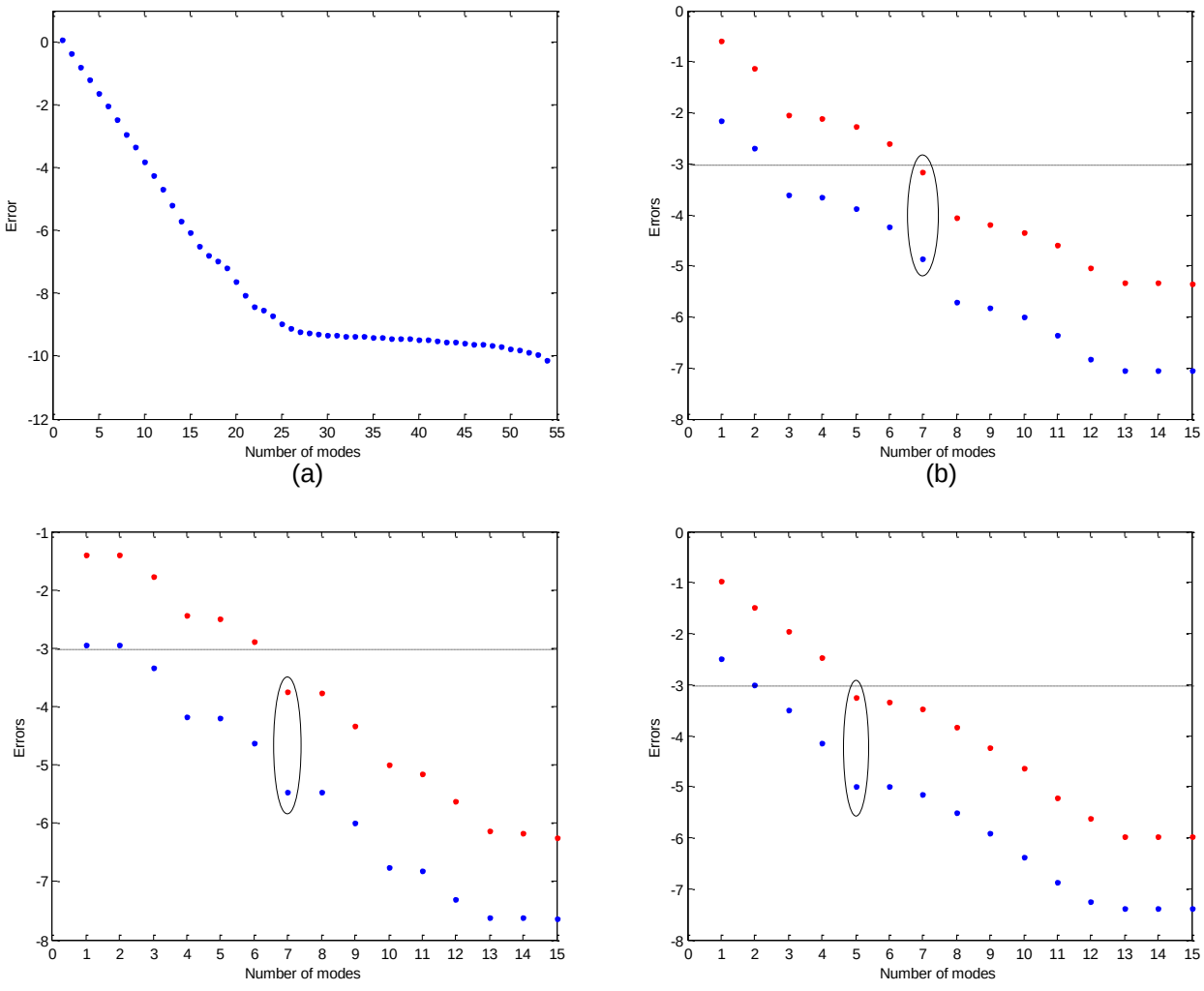

Fig. 5.4 RMS errors vs. the number of retained modes using 55 equispaced snapshots . (a) Global error for 54 test case; (b) error for Re = 55, (c) error for Re = 455, and (d) error for Re = 955.

For the sake of clarity three cases are considered, using 55, 22, and 11 equispaced snapshots. For each of these three cases, the error is calculated for various numbers of retained modes in the reconstruction of the solution, at three different values of the Reynolds number, one at the beginning of the selected range, which goes from 10 to 1100, another in the middle of the range and a final one at the end of it.

The case of 55 snapshots is considered in figure 5.4. The first plot provides the global RMS error in reconstructing the 54 test cases considered above, and the remaining three plots, the errors for the above mentioned values of the Reynolds number. These plots suggest that 7 modes are enough in this case to reconstruct the solution for the three selected values of the Reynolds number. However, 55 snapshots are too many, as already noticed. Thus, the dependence of the number of required modes on the number of snapshots needs to be analyzed.

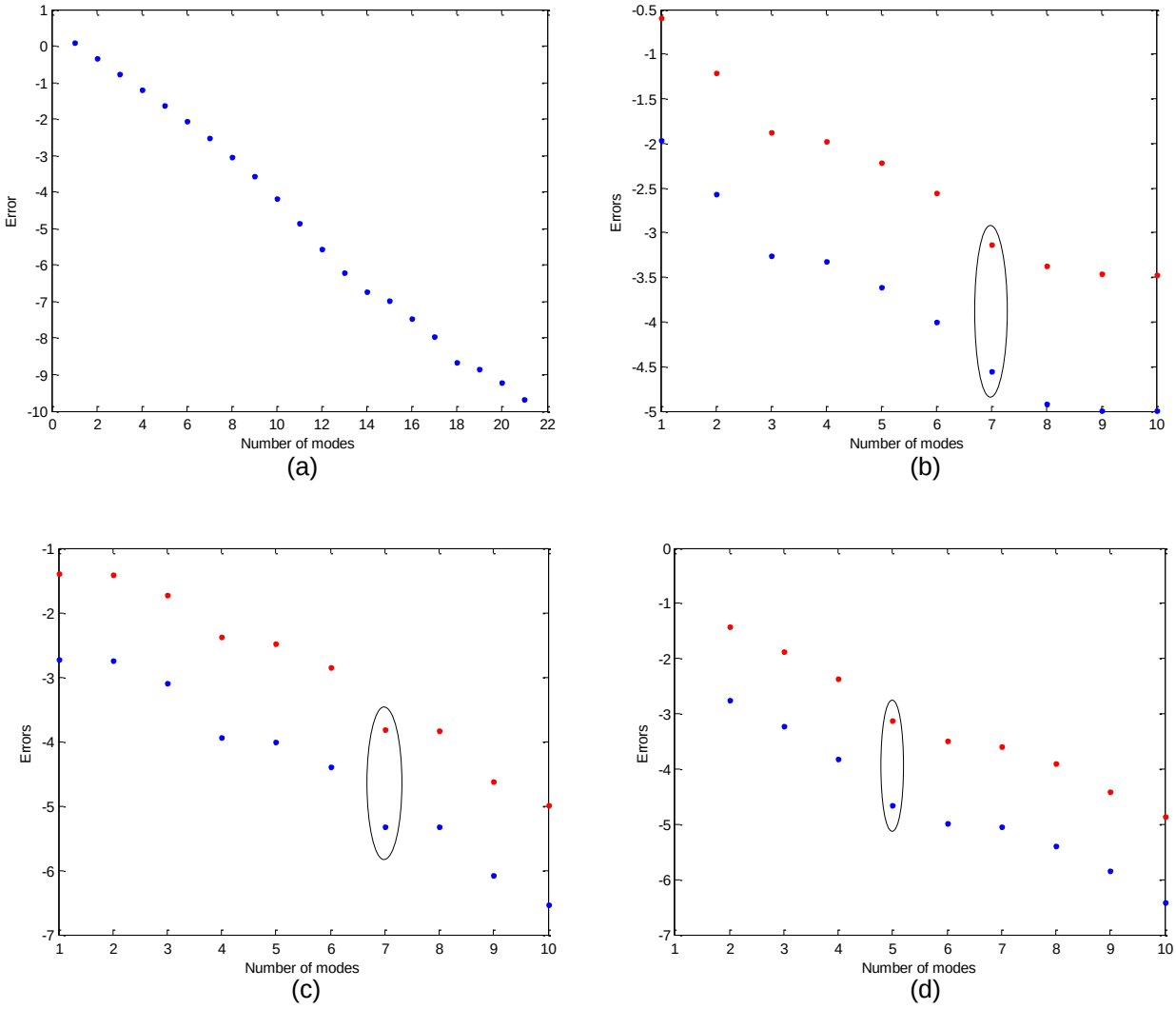

Fig. 5.5 Counterpart of figure 5.4 using 22 snapshots.

The case of 22 equispaced snapshots is considered in figure 5.5, which shows that 7 modes are also enough if 22 equispaced snapshots are used. This emphasizes the fact that 55 snapshots are quite redundant.

However, as seen in figure 5.6, if the number of snapshots is again reduced to the half, 11 equispaced snapshots, then for some values of the Reynolds number the model does not reach the steady state with a maximum error of 10^{-3}. This is because the information provided by only 11 snapshots is not enough to build an efficient model.

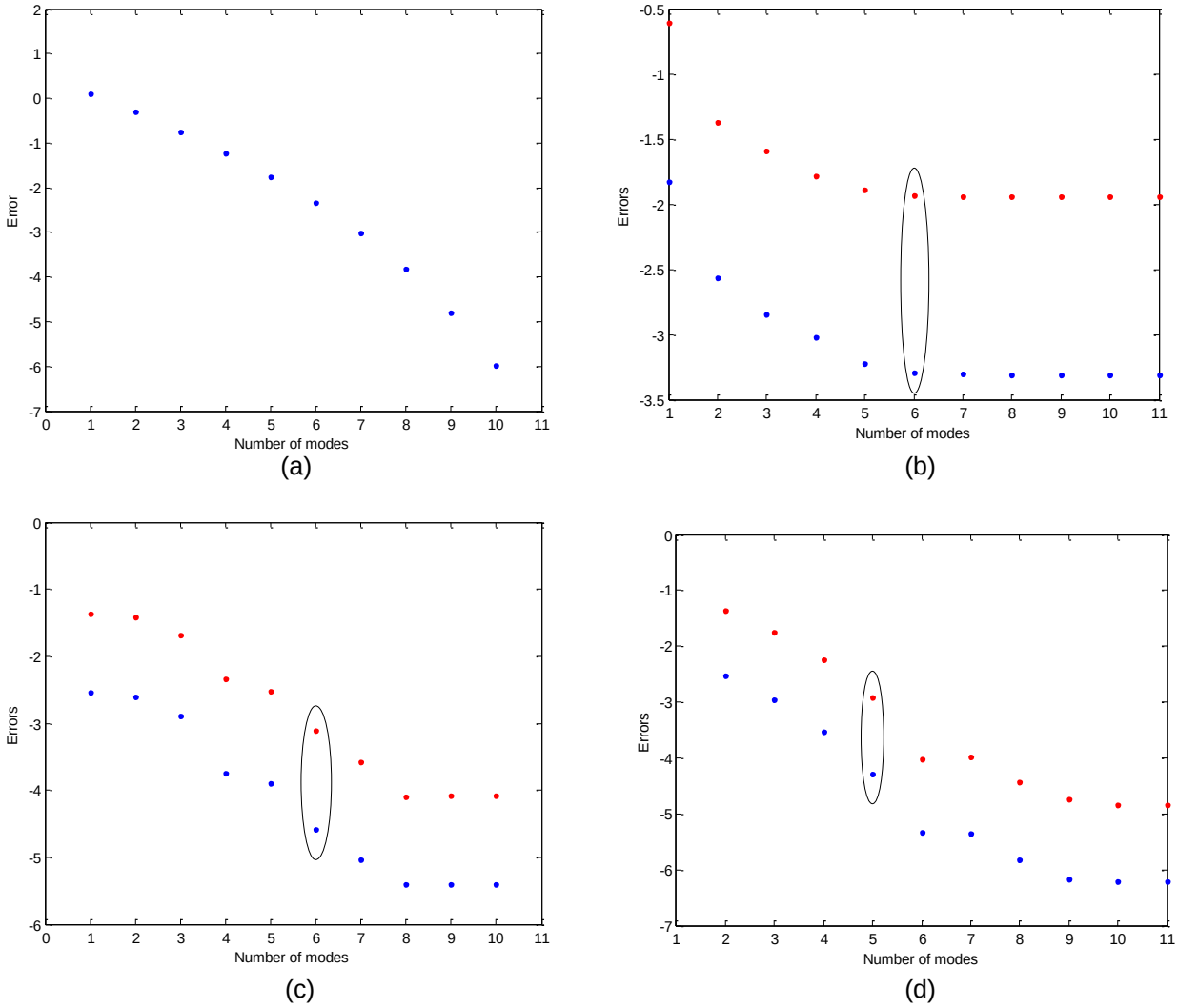

Fig. 5.6. Counterpart of figure 5.4 using 11 snapshots.

Summarizing these results, the error of the method is due to both truncation in the SVD step and interpolation. The number of snapshots should be enough to both produce sufficiently good spatial modes and prevent interpolation errors. Increasing the number of snapshots from this threshold level, does not produce any additional benefit and decresing the number of snapshots worsen both the quality of the modes and the efficiency of the interpolation. Of course, the location of the snapshots in the Reynolds number range matters, but this is outside the scope of this dissertation.

Chapter 6

APPLICATION OF HOSVD TO THE LID-DRIVEN CAVITY PROBLEM

6.1. Application of HOSVD to the lid-driven cavity problem

Higher-order tensor (*N*-array with $N \geq 3$) decompositions are applied in many different areas such as psychometrics, signal processing, numerical linear algebra, computer vision, numerical analysis, neuroscience or graph analysis among others (see [17]).

Several of these decompositions have been studied for long (see [17] and [18]). However, since in the one-parameter dependence problem the method used was based on POD and/or SVD, the decomposition called High Order Singular Value Decomposition is the one to be used for multiparameter problems. But not only the resemblance of POD and HOSVD, which can be seen as an extension to third order tensors of SVD, made us chose this decomposition, also the knowledge of the good results provided when applied to problems that are genuinely multidimensional (see [1]).

Since no additional parameters are available in the lid-driven cavity, in order to apply High Order Singular Value Decomposition to the problem of the lid-driven cavity, it is necessary to reorder the snapshots in a way that simulates the multi-parameter dependence. This is carried out by dividing the Reynolds number range in two scales, which will be called the long scale, which gives the order of magnitude of the Reynolds number, and the short scale, which specifies the actual values of Reynolds number in each interval of the long scale. In order to do this is, the whole range of the Reynolds number will be divided into sub-ranges of the same length, this is the long scale division, which will be accounted for with third index of the tensor, k. After this, the second index accounts for the short range, namely the position of the Reynolds number in the k-th subinterval of the long range. Finally, the first index stands as it was before, it labels the various points of the spatial mesh.

An example is given for the sake of clarity. Suppose that the 110 steady state solutions corresponding to Reynolds numbers taken from 10 to 10, between 10 and 1100 are provided. First, the Reynolds interval [1, 1100] is divided in eleven subintervals, [1, 100], [101, 200], …, [1001, 1100]. Then the long scale index varies from 1 to 11 indicating in which of these subintervals is located the Reynolds number. Note that the same number of snapshots must be contained in each one of these subintervals; in other words, the same number of Reynolds for which the solution is known. In our case, ten snapshots are given in each subinterval, so the short scale index goes from 1 to 10. Finally, index i continues going from 1 to 2 x 33 x 33, which is twice the dimension of the selected mesh.

Along this chapter, we refer to the third order $(m\ x\ n\ x\ p)$- tensor, whose elements are given by A_{ijk} as the ***snapshots tensor***.

When HOSVD is applied, three kinds of modes are obtained, which are associated with the three dimensions. The first one corresponds to the spatial mesh and thus the associated modes are the spatial modes, which are independent of the Reynolds number. The second and third indexes give the long and short scales and the associated modes can be seen as respectively long range and short range parametric modes. The core tensor is independent of both the spatial and parametric indexes. Thus, if an intermediate value of the Reynolds number is to be considered, then interpolation must be made only in the short range parametric modes, once the long range value of the index has been identified. As above, interpolation will be made using cubic splines.

6.2. Global Error

As described in section 3.4, the error introduced by HOSVD when truncating to $\tilde{m}\ x\ \tilde{n}\ x\ \tilde{p}$, where $\tilde{m} \le m,\ \tilde{n} \le n$ and $\tilde{p} \le p$ can be bounded by the expression **(3.31)**. The dependence of the global error on the 3 sets of eigenvalues, instead of just one as it happened when dealing with POD (or SVD), makes it a bit harder to study the global error of the method. In fact, **(3.31)** provides us with just an upper bound of the error.

Figure 6.1 shows the dependence of the error with the number of modes taken in each of the three orthonormal sets. Each of the plots shows the dependence on a different index. For the first case, plot (a), the modes are taken for second and third indexes, while the number of modes taken for the first index changes from 1 to the total number of them (m = 2 x 33 x 33). In figure 6.1 (b), the error when varying the number of modes taken for the second index is plotted, while for the first and third indexes, all the modes are retained (that is $\tilde{m} = m$ and $\tilde{p} = p$). Finally, the counterpart is done in plot (c), where $\tilde{m} = m$ and $\tilde{n} = n$, and $\tilde{p}$ varies from 1 to p (in this case p =11). A bound for the global error is given by the sum of the 3 errors. It is observed that the biggest reduction is obtained from the first index.

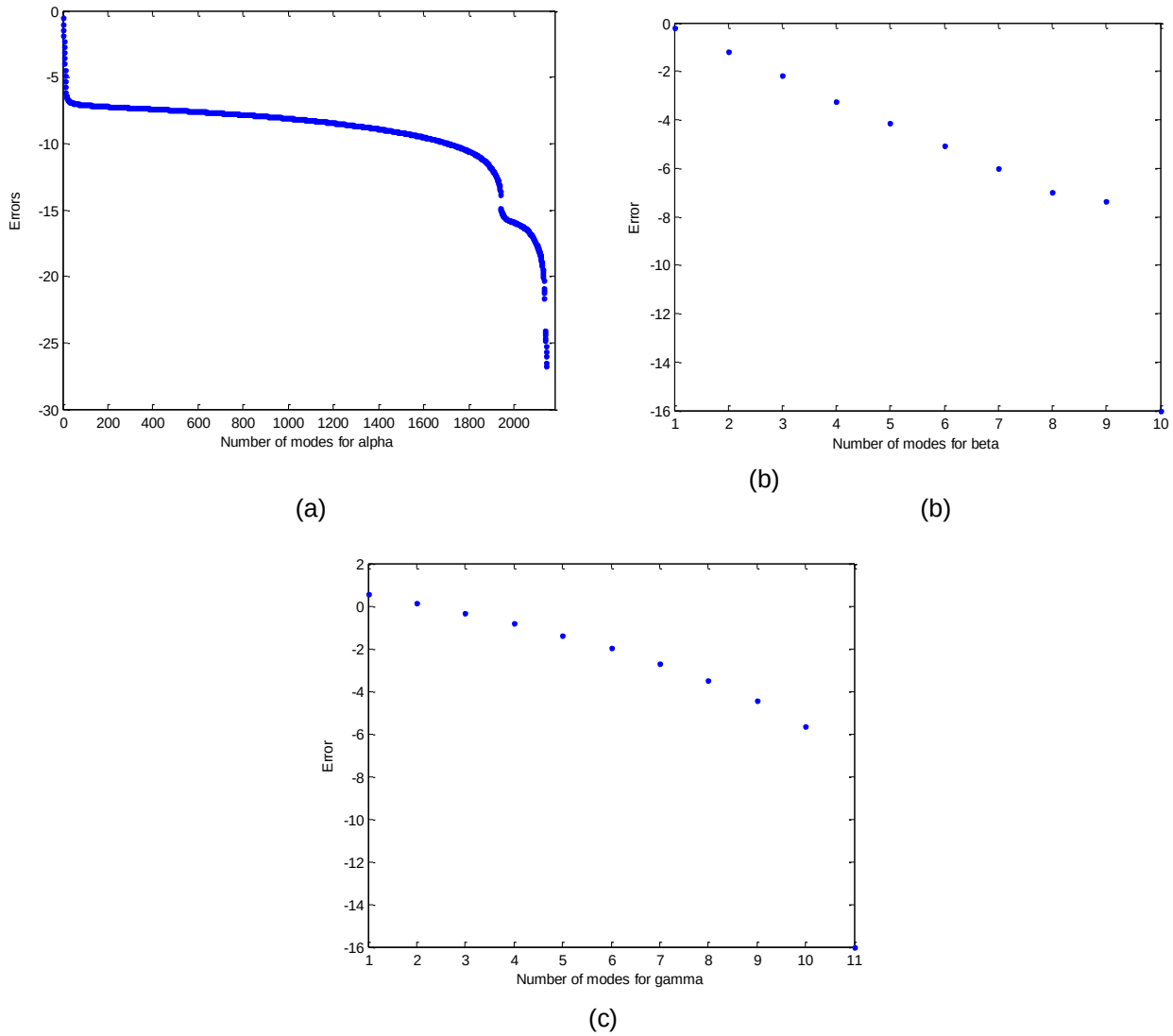

Fig. 6.1 Error of the method depending on the number of modes taken for (a) the first index, (b) the second index, and (c) the third index of the tensor, when taking all the modes for the other two indexes. Errors are given in logarithmic scale and the case treated is that of 110 snapshots provided.

Assume that the three orthonormal systems of eigenvalues, and their associated eigenvectors, are ordered such that the most energetic one is located first and then in decreasing order. The global dependence of the error on the number of modes taken can be studied in the following way. First, the error of the method when retaining just one *HOSVD* mode in each of the three sets (u_1, v_1 and w_1) is calculated. These first modes correspond to the most energetic eigenvalue of each one of the three systems (α_1, β_1 and γ_1). Then, a new mode is selected to be added to the retained ones and the error of the new system is calculated. The selection of this new mode is made with respect to the most energetic eigenvalue left, thus either a mode can be added for the first system (u_2) if $\alpha_2 > \beta_2$ and $\alpha_2 > \gamma_2$, or for the second system (v_2) in case of being $\beta_2 > \alpha_2$ and $\beta_2 > \gamma_2$, or for the third system (w_2)

if $\gamma_2 > \alpha_2$ and $\gamma_2 > \beta_2$. This process goes on adding one mode at a time and calculating the error of the model for the total number of modes retained, until all of them have been selected. In that way, if in the second step $\alpha_2 > \beta_2$ and $\alpha_2 > \gamma_2$, then a HOSVD mode for the first of the orthonormal systems is retained and the error of the method retaining those four modes (u_1, v_1, w_1 and u_2) is obtained. However, it is of no interest to retain all the modes. The interest of the process is to retain the least number of modes possible for a given error, then instead of adding modes until the total number of them is taken, the process is stopped when an error smaller than a given value is reached.

From now on, a (2178 x 5 x 11)-tensor is considered, unless otherwise stated. This tensor corresponds to the case of 55 snapshots given. The dependence of the error of the model with respect to the total number of modes taken is plotted in figure 6.2. In addition, the corresponding numbers of modes of each one of the three orthogonal systems of eigenvectors are shown in table 6.1. Considering the obtained data, in order to calculate the solution for a Reynolds number in the given range with an error less than 10^{-5}, it is enough to retain 26 HOSVD modes, from which 12 are taken from the first system, 5 from the second (these are all of them) and 9 (over the 11 possible) from the third.

In order to compare the model obtained using HOSVD with the one obtained for the POD/SVD, let us fix the bound for the error to 10^{-3}. For the HOSVD-based method (with 55 snapshots), in order to calculate the solutions of the problem for any Reynolds in the given range with an error smaller than 10^{-3}, it is necessary to retain 18 modes (8 from *U*, 3 from *V* and 7 from *W*). In contrast, for the case of POD-based model it was enough to retain 7 modes. This fact leads us to think, without further exploration of the methods, that the HOSVD-based model is not as good as the POD-based one. However, previous studies on related problems (see [1]) drives us to think that HOSVD-based models provides good results in cases in which the problem is genuinely multidimensional.

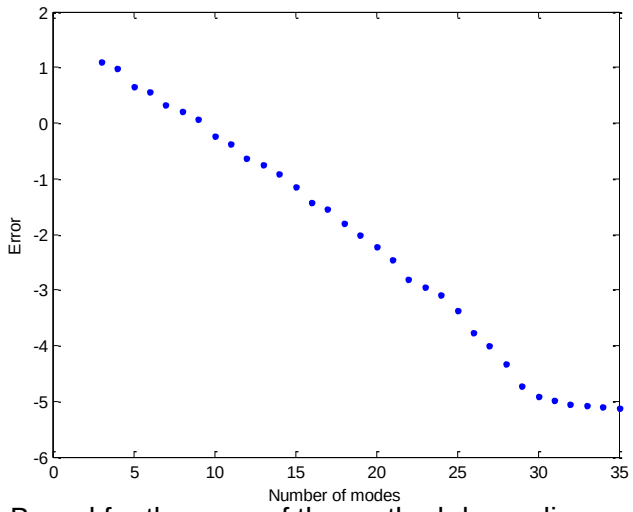

Fig. 6.2 Bound for the error of the method depending on the number of modes, for a (2178 x 5 x 11) – tensor

Table 6.1: Table of modes

total modes	3	4	5	6	7	8	9	10	11	12	13	14	15	16	17	18	19	20	21	22	23	24	25	26	27	28	29	30	31	32
U	1	1	2	3	3	3	4	4	5	5	6	6	6	7	7	8	8	9	9	10	11	11	11	12	13	13	14	15	16	16
V	1	1	1	1	1	2	2	2	2	2	2	3	3	3	3	3	4	4	4	4	4	4	5	5	5	5	5	5	5	5
W	1	2	2	2	3	3	3	4	4	5	5	5	6	6	7	7	7	7	8	8	8	9	9	9	9	10	10	10	10	11

6.3. Interpolation error

Interpolation is made over the retained modes. In fact, it is done over the modes for the short scale associated system (*V*).

To compare with the results obtained for the POD-based model, the cases corresponding to those shown in figure 5.4 are plotted in figure 6.3. Different ideas are seen in this figure. On the one hand, in plot (a), the bound for the error, given by the sum of the singular values, is plotted in blue dots and the maximum error obtained when reproducing the snapshots in red dots, both depending on the number of modes retained. On the other hand, the other three plots show the maximum error obtained, depending on the number of modes retained, when calculating the solution for (b) Re = 55, (c) Re = 455, and (d) Re = 955.

The minimum number of modes for which the obtained solutions give maximum errors smaller than 0.001 is 16. This can be also observed in figure 6.2. Thus, the number of modes needed using the HOSVD-based model, to calculate the steady state solutions of the lid-driven cavity problem, is higher than the number needed for POD-based models.

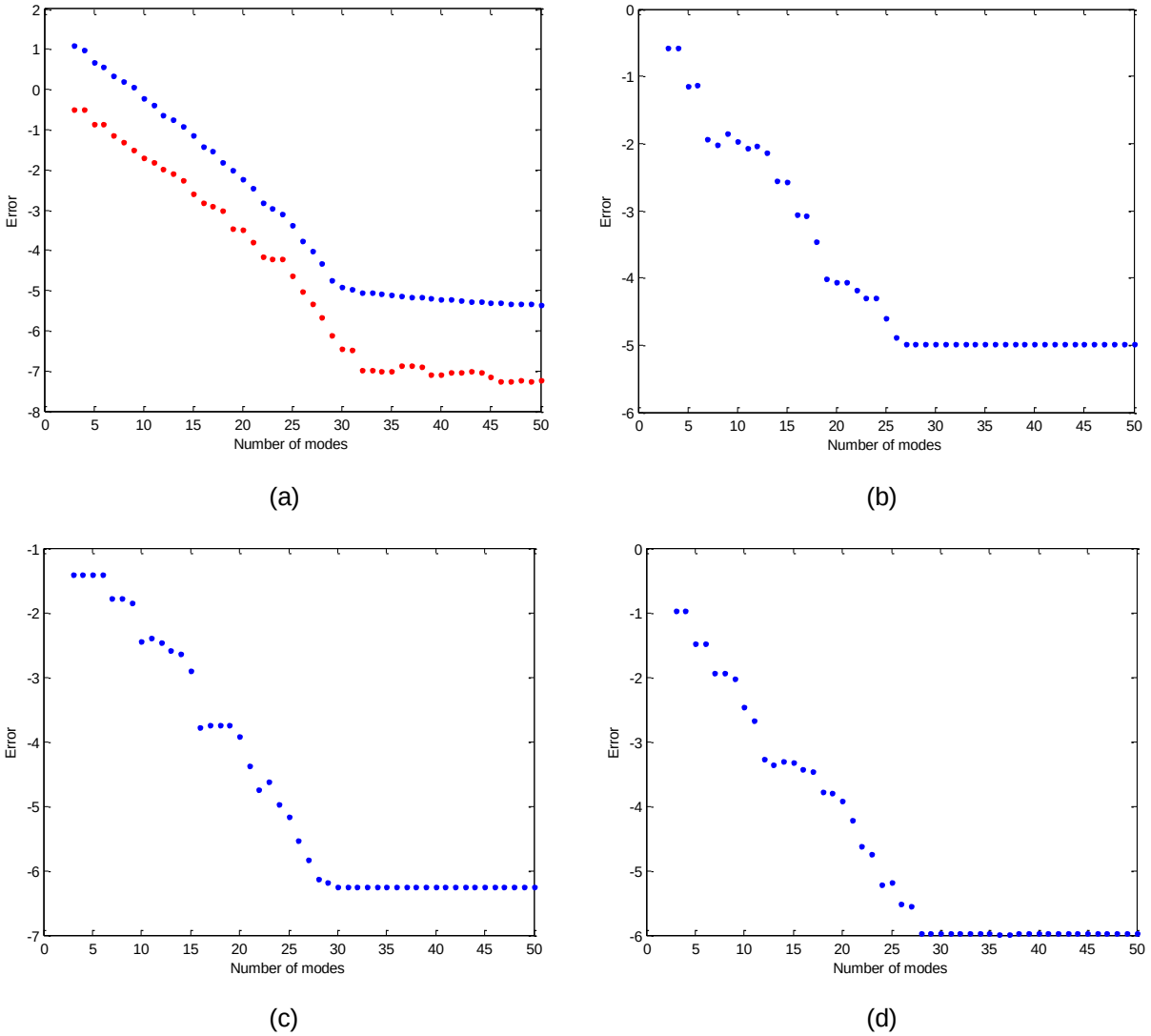

Fig. 6.3 Plot (a) Bound for the error of the model (blue dots) and maximum error when reproducing the snapshots (red dots) both depending on the number of modes taken. Plots (b), (c) and (d) show the maximum errors from calculating the solutions for Reynolds numbers 55, 455 and 955 (respectively) depending on the number of modes retained. All the errors are given in logarithmic scale.

Chapter 7

CONCLUSIONS AND FUTURE DEVELOPMENTS

7.1. Summary

A model has been proposed to accelerate the calculation of the steady state solutions of the lid-driven cavity problem. The model begins with the application of Proper Orthogonal Decomposition to a set of steady state solutions, which are obtained using a CFD code. This decomposition gives the best *n*-dimensional approximation of the sample set (by selecting the *n* more energetic POD modes), for any *n* less or equal to the number of solutions provided. Afterwards, the given solutions are projected onto the set of modes retained to obtain the coefficients (amplitudes) which, when multiplied by the modes, give that best *n*-dimensional approximation to the solution.

In fact, the RMS error of this procedure when *n* POD modes have been retained is easily obtained, which makes easy to find out how many of the modes are necessary to calculate the solutions of the problem within a given error, after having the first contact with the method.

The solutions for a new value of the Reynolds number are obtained by interpolation on the amplitudes of the retained modes. However, with the interpolation some errors are introduced in the model.

With the available numerical code, the computational time expended to calculate these solutions for some values of Reynolds numbers is shown in table 7.1. As it can be observed, the computational time increases with the Reynolds number.

Table 7.1 Time expended by the numerical code

Reynolds	10	100	300	500	700	900	1100
Comp.Time (s)	57	99	229	303	410	535	664

In contrast, the reduced model presented in this work allows to obtain any steady state solution almost instantaneously (namely, within around 1.5 seconds). In fact, the CPU time used to calculate any steady state solution does not depend on the Reynolds number.It is invariant once the number of modes retained is selected.

7.2. Conclusions

The model proposed here is able to calculate the steady state solution for any Reynolds number in the interval [1, 1100] within a maximum error of 10^{-3}. In fact, an

approximation (within a given error) of the steady state is obtained even when a small number of snapshots are provided.

Several cases were studied more in detail during chapter 5 to illustrate the results obtained, which are summarized here. On the one hand, if the number of snapshots provided is too large, a small number of POD modes is necessary to calculate new solutions. In fact, the number of POD modes needed does not vary while the number of snapshots provided is large. However, if the number of snapshots given is not enough, it is possible that a big amount of information is lost when one single mode is not retained.

On the other hand, there is the need to take into account the interpolation errors. These errors are greater as less information is provided; in other words, the interpolation error will be greater as fewer snapshots are provided.

It is observed that provided 22 snapshots, for a maximum error of 10^{-3} it is enough to retain 7 POD modes. In conclusion, the model is efficient both in terms of time-costs and in terms of its effectiveness to calculate the steady state solution of the problem within a given error.

At the end of this thesis the model has been compared with a HOSVD-based one. An improvement was expected when using this more sophisticated idea, but the results obtained were not that good; more time is spent to calculate the solutions and more snapshots and modes are necessary. On the one hand, this drives us to think that the long and short scales used for the Reynolds number (in order to transform the one-parameter dependence in multi-parameter) is not good and better results could be obtained if re-scaling in a different way. It could also be better to simulate the dependence on more than one parameter in another way, such as the dependence of the solution in the points of the grid (x, y).

7.3. Future developments

Methods based on POD are seen to be very efficient. Future developments related with the work carried out here should begin with the extension of the range in which the Reynolds numbers have been selected. However, the application of the model to other problems is also a work that should be done.

With respect to the HOSVD, models based on this idea normally give good results. As previously commented, it is possible that the problem here was the scales chosen. Several ideas of future works are given here, among which the more important ones are those in which the problem depends in more than one physical parameter.

First cases to carry out can be to open the given range for the Reynolds numbers and change the long and short scales. Another idea could be to choose another way to “reproduce” the multi parametrical dependence, for instance, instead of giving all the information for a Reynolds number in a column, make it occupy a whole matrix. In other words, first separate the stream function and vorticity solutions in two different problems. Then, for each Reynolds, it is possible and more natural to give the

solution in a 33 x 33 matrix, where one of the indexes of the matrix accounts for the x-points of the grid and the other for the y-points. The element A_{ij} of the matrix gives the stream function (or vorticity) for the steady state solution of the problem at the point (x_i, y_j) of the grid. Finally, this can be easily extend to a tensor where the third index accounts for the different Reynolds numbers.

However, the best thing is to account for a real multi-parameter dependence, for example changing the shape of the cavity. If the work is done for rectangular cavities with base (l) and height (h), apart from the Reynolds number, the problem could depend on the relation over the base and the height.

References

[1] Lorente, L.S., Vega J.M. and Velazquez, A. “Generation of Aerodynamic Databases Using High-Order Singular Value Decomposition”. *Journal of Aircraft*. 45(5), 1779–1788 (2008).

[2] Lorente, L.S., Vega J.M. and Velazquez, A. “Compression of aerodynamic databases using High-Order Singular Value Decomposition”. *Aerospace Science and Technology* 14, 168-177 (2010).

[3] Alonso, D., Velazquez, A. and Vega J.M. “Robust reduced order modeling of heat transfer in a back step flow”. *International Journal of Heat and Mass Transfer* 52, 1149-1157 (2009).

[4] Bui-Thanh, T., “Proper Orthogonal Decomposition Extensions and their Applications in Steady Aerodynamics,” Master´s Thesis, Singapore-Massachusetts Institute of Technology Alliance, 2003.

[5] Rapún, M.L. and Vega, J.M., “Reduced order models based on local POD plus Galerkin projection”, *Journal of Computational Physics*, 229(8), 3046-3063 (2010).

[6] Liang, Y. C., Lee, H.P., Lim S.P., Lin, W. Z., Lee, K. H. and Wu, C.G., “Proper Orthogonal Decomposition and its Applications – Part I: Theory,” *Journal of Sound and Vibration* 252(3), 527-544 (2002).

[7] Klema, V. C. and Laub, A. J., “The Singular Value Decomposition: Its Computation and Some Applications,” *IEEE Transactions on Automatic Control* AC-25, No. 2, 164-176 (1980).

[8] De Oathauwer, L., De Moor, B., and Vandewalle, J., “On the Best Rank-One and Rank-(R_1, R_2, …, R_N) Approximation of Higher Order Tensors,” *SIAM Journal on Matrix Analysis and Applications*, 21(4), 1324-1342 (2000).

[9] Da Silva, V. and Lim, L., “Tensor rank and the ill-posedness of the best low-rank approximation problem,” *SIAM Journal on Matrix Analysis and Applications*, 30, 1084-1127 (2008).

[10] Burggraf, O. R., “Analytical and numerical studies of the structure of steady separated flows”, *Journal of Fluid Mechanics* 24(1), 113-15 (1966).

[11] Ghia,U. , Ghia, K. N. and Shin, C. T. “High-Re solutions for incompressible flow using the Navier–Stokes equations and a multigrid method”. *Journal of Computational Physics* 48, 387-411 (1982).

[12] Botella, O. and Peyret, R., "Benchmark spectral results on the lid-driven cavity flow" , *Computers and Fluids*, 27(4) , 421-433 (1998).

[13] Theofilis, V. "Advances in global linear instability analysis of nonparallel and three-dimensional flows" *Progress in Aerospace Sciences,* 39, 249-315 (2003).

[14] Sparlat, P.R., Moser, R.D. and Rogers, M.M., "Spectral methods for the Navier-Stokes equations with one infinite and two periodic directions" *Journal of Computational Physics* 96, 297-324 (1991).

[15] De Jesús Martinez, J. and de Tarso, P., "A Chebyshev Collocation Spectral Method for Numerical Simulation of Incompressible Flow Problems", *Journal of the Brazilian Society of Mechanical Sciences and Engineering,* 29(3), 317-328 (2007).

[16] Canuto, C., Hussaini, M., Quarteroni, A. and Zang, T.A., *Spectral Methods. Evolution to Complex Geometries and Applications to Fluid Dynamics*, Ed. Springer-Verlag, Berlin (2007)

[17] Kolda, T.G., and Bader, B.W., "Tensor Decompositions and Applications", SIAM. Rev. 51 455-500 (2009).

[18] De Lathauwer, L., De Moor, B. and Vandewalle, J. "A multilinear singular value decomposition", *SIAM. Journal of Matrix Analysis and Applications*, 21, 1324-1342 (2000).